Accepted article in the Journal of Inorganic Biochemistry: 2.22.2022

Interactions of *N*-hydroxyamphetamine with an iron porphyrin: A unique intramolecular H-bond probed by DFT calculations

Ye Guan, Jennifer Londoño-Salazar, Zheng Pei, Douglas R. Powell, Yihan Shao, and George B. Richter-Addo**

Price Family Institute of Structural Biology and Department of Chemistry and Biochemistry
University of Oklahoma
101 Stephenson Parkway, Norman, OK 73019
E-mail: yihan.shao@ou.edu, grichteraddo@ou.edu

Abstract: Hydroxylamine (NH_2OH) and its *N*-substituted derivatives (RNHOH) are important biological intermediates in the global N cycle. Heme plays a central role in the binding and activation of these hydroxylamines. We report the crystal structures of *N*-hydroxyamphetamine (AmphNHOH) in complex with Fe and Co heme models. We demonstrate a previously unrecognized internal H-bond interaction between a hydroxylamine RNH*O–H* group and a porphyrin N-atom. We utilize density functional theoretical (DFT) calculations to show that the conformations with the internal H-bond represent global minima along the potential energy surfaces for both the Fe and Co heme models. A natural bond orbital (NBO) analysis reveals a donor π ($por_{N=C}$) to acceptor π^* (O–H) interaction of 3.04 kcal/mol for Fe, accounting for 11% of the total heme–AmphNHOH interaction energy. Our DFT calculations with the parent Fe–NH_2OH suggests that the presence of internal H-bonds between hydroxylamine (R/H)NH*OH* moieties and heme N-atoms may be more common than previously recognized.

Keywords: porphyrin • X-ray structure • density functional calculations • hydroxylamine • iron

1. Introduction

N-hydroxyamphetamine (AmphNHOH) is a product of amphetamine ($AmphNH_2$) metabolism in mammals [1, 2]. Extensive studies on the metabolism of $AmphNH_2$ and methamphetamine in humans and other mammals have been reported [3, 4]. For example, human cyctochrome P450 2D6 metabolizes methamphetamine to $AmphNH_2$ and its oxidative products *N*-hydroxymethamphetamine and *p*-hydroxymethamphetamine [3]. Interestingly, a flavin-containing monooxygenase FMO3 in humans also metabolizes $AmphNH_2$ to AmphNHOH [5]. Once generated, AmphNHOH can be converted by several pathways to the nitroso derivative AmphNO (Figure 1).

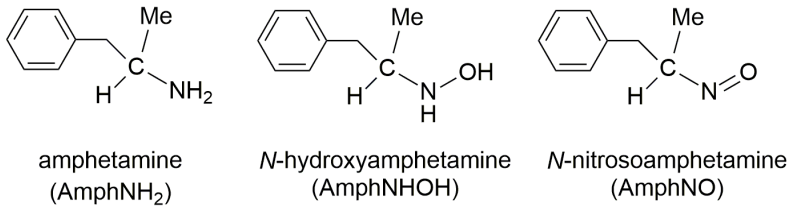

Fig. 1. Amphetamine and selected oxidative metabolites.

It is known that AmphNHOH, once generated, interacts with the heme sites of some heme proteins to form inhibitory nitroso Fe^{II}–N(O)Amph derivatives that essentially shut down protein function [6-9]. We reported the X-ray crystal structures of the Fe^{II}–N(O)Amph derivatives of tetrameric human hemoglobin [10] and a sperm whale mutant H64A myoglobin [11], in which the AmphNO ligands were bound to Fe via the nitroso N-atom. Despite the recognition of AmphNHOH as an important metabolite in heme-based $AmphNH_2$ metabolism, no X-ray crystal structure of a heme–AmphNHOH complex (protein or heme model) has been reported to date.

The parent hydroxylamine NH_2OH is also biologically important [12-15]. It is a substrate for the P460 heme in the multi-heme enzyme hydroxylamine oxidoreductase (HAO) [16-18]. In addition, it is an intermediate in the enzymatic six-electron reduction of nitrite to ammonia by cytochrome *c* nitrite reductase (cyt *c* NiR) [19], and is an intermediate in biological hydrazine synthesis from nitric oxide (NO) by a multi-heme hydrazine synthase complex [20]. Importantly, heme-based metabolism of NH_2OH can be either oxidative (e.g., to generate NO) or reductive (e.g., to generate NH_3). Four X-ray crystal structures have been reported for heme protein–NH_2OH adducts, namely those of cytochrome P460 from the ammonium oxidizing bacterium *nitrosomonas sp.* AL212 (at 2.25 Å resoln.) [17], cyt *c* NiR from *W. succinogenes* (at 2.0 Å resoln.) [19], assimilatory NiR from tobacco (at 1.3 Å resoln.) [21], and a class II peroxidase from *Arthromyces ramosus* (at 1.3 Å resoln.) [22]. Although the resolutions of these structures do not allow unambiguous locations of the NH_2OH H-atoms, the active site distal pocket makeup in these protein structures have allowed the formulation of varied extents of distal pocket H-bond interactions as shown in Figure 2.

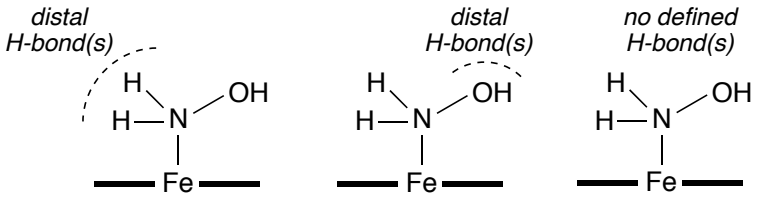

Fig. 2. Sketches of the H-bond interactions for the heme-NH_2OH adducts of P460 (left), cyt *c* and siroheme NiR (middle), and peroxidase (right).

With regard to heme model compounds, Ryan and coworkers have reported the reactions of NH_2OH with ferric (TPP)FeCl and ferrous (TPP)Fe at low temperature (e.g., –40 °C) to give ferrous (TPP)Fe$(NH_2OH)_2$ species that decompose at room temperature to (TPP)Fe(NO) [23].

Density functional theory (DFT) calculations on both truncated heme protein–NH_2OH and heme model–NH_2OH systems have aided immensely to help elucidate the complex mechanisms of NH_2OH metabolism. For example, systems studied include low-spin ferric P460 [24], ferric and ferrous cyt *c* NiR [19], and a non-protein ferric (porphine)Fe(NH_2OH)(Imd) model [25]. These studies reveal, to date, the conventional □-bonding between the N-atom of NH_2OH and the Fe centers as the sole interaction between the heme and NH_2OH. Unfortunately, no X-ray crystal structures of heme model–NH_2OH or –RNHOH (R – alkyl, aryl) have been reported to date, thus hampering further studies in this area [26-31].

Although heme is involved in RNHOH/NH_2OH metabolism, it is not entirely clear if there are unique features (in addition to active site distal pocket interactions) of the heme macrocycle that could contribute towards heme-mediated RNHOH/NH_2OH binding and activation. In this paper, we report the first X-ray crystal structures of metalloporphyrin-alkylhydroxylamine complexes, namely those containing Fe–AmphNHOH and Co–AmphNHOH linkages. We utilize DFT calculations to probe the experimental observation of an unprecedented internal H-bond between the hydroxy –OH groups of the bound AmphNHOH ligands and porphyrin N-atoms. Our extensions to the parent NH_2OH in a non-protein heme model reveal the presence of similar internal H-bonds between the hydroxylamine –OH group and a porphine N-atom. This suggests that, in the absence of competing distal pocket H-bonding interactions between bound RNHOH/NH_2OH groups and distal residues, such internal H-bonding might need to be addressed when considering factors that contribute to the activation of RNHOH/NH_2OH ligands by heme.

2. Results and Discussion

Reactions of the ferric precursor (OEP)FeCl with excess N-hydroxyamphetamine (AmphNHOH) followed by addition of 1-MeIm results in the formation of the nitrosoamphetamine adduct (OEP)Fe(AmphNO)(1-MeIm) in 58% isolated yield (eq. 1). This

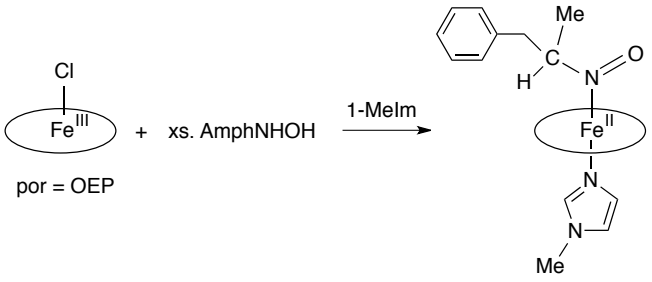

(1)

reaction is not unlike those reported earlier by Mansuy [32] and by us [33] for other nitrosoalkane derivatives, with the formation of the nitroso product likely being enhanced by the presence of trace air. A new band in the IR spectrum of (OEP)Fe(AmphNO)(1-MeIm) is consistent with the formulation of the amphetamine metabolite as a nitroso derivative; c.f., ν_{NO} at 1423 cm^{-1} for (OEP)Fe(*i*-PrNO)(1-MeIm) [33]. The crystal structure of the (OEP)Fe(AmphNO)(1-MeIm) product is shown in Figure 3. The Fe–N(O) distance of 1.806(6) Å is shorter than the *trans* Fe-N(1-MeIm) distance of 2.067(5) Å, and is consistent with the nitroso ligand being a π-acid in this complex. Although two heme protein-AmphNO structures are known, namely those of Hb(AmphNO) [10] and H64A Mb(AmphNO) [11], this is the first heme model-AmphNO structure to be reported. As with the Hb and Mb derivatives, only the *d*-isomer of AmphNO was present in the crystal structure. The AmphNO ligand exhibits an 82:18 disorder, with the major nitroso CNO component bisecting an adjacent pair of porphyrin N-atoms (τ N1–Fe1–N7–O1 torsion angle of 47.7(5)°). The axial 1-MeIm ligand essentially eclipses a pair of porphyrin diagonal N-atoms.

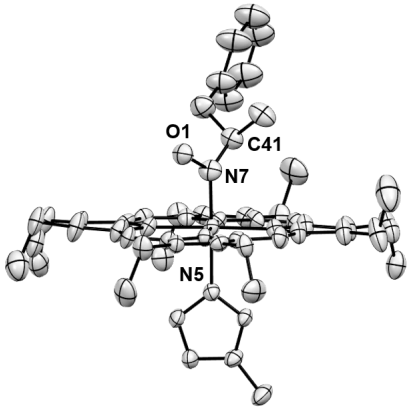

Fig. 3. Molecular structure of (OEP)Fe(AmphNO)(MeIm) showing only the major (82%) disordered AmphNO component (nitroso N7 is ordered). Selected bond lengths and angles: Fe1–N7 = 1.806(6) Å, N7–O1 = 1.318(7) Å, N7–C41 = 1.434(10) Å, Fe1–N5 = 2.067(5) Å, Fe(1)–N(por) = 1.989(5)–2.019(5) A, ∠Fe1–N7–O1 = 120.2(5)°, ∠Fe1–N7–C41 = 126.1(5)°, ∠N7–Fe1–N5 = 178.9(2)°, ∠N1-Fe1-N7-O1 = 47.7(5)°. Hydrogen atoms have been removed for clarity. Thermal ellipsoids are drawn at 50%.

The geometrical data for the AmphNO moiety are not unlike those of other Fe-nitrosoalkane complexes, and will not be commented on further.

In our quest to obtain an isolable intermediate for this alkylhydroxylamine-to-nitroso reaction, we were fortunate to obtain suitable crystals of the product from the reaction of (TPP)FeCl with AmphNHOH in the absence of added base (eq 2).

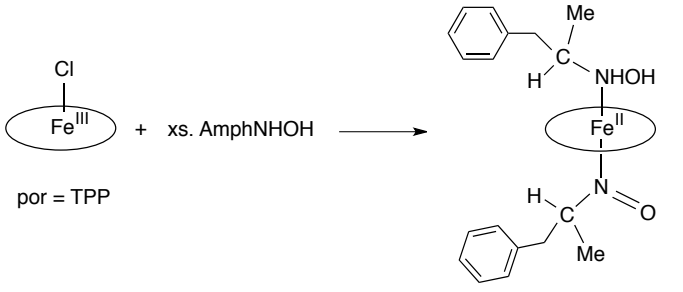

(2)

The crystal structure of this air-sensitive intermediate was obtained and identified as the six-coordinate (TPP)Fe(AmphNHOH)(AmphNO) complex (Figure 4A) which was isolated in ~40% yield. Selected geometrical data are listed in the caption and in Table 1.

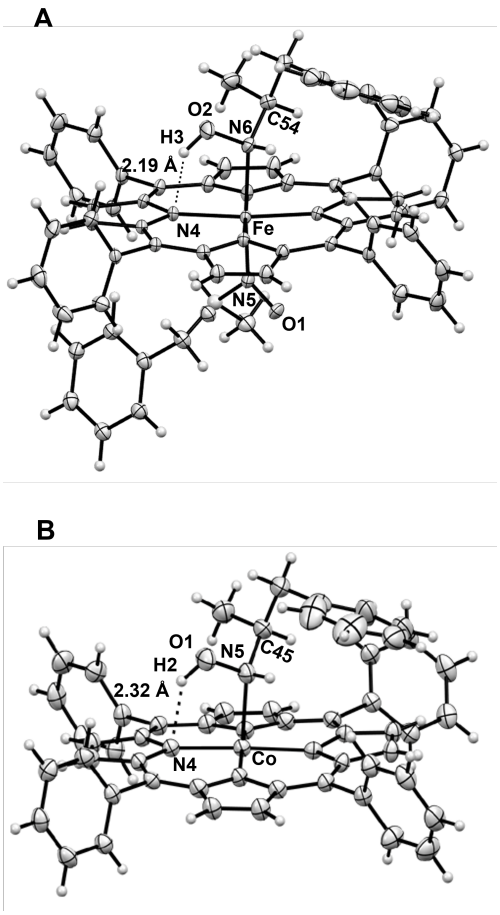

Fig. 4. (A) Molecular structure of (TPP)Fe(AmphNHOH)(AmphNO). The two H atoms of the –NHOH moiety were located in the difference electron density map, and the H-bond between the porphyrin N4 atom and the NOH proton (H3) is represented by a dashed line (2.19 Å). Geometrical data for the Fe-AmphNHOH moiety are shown in Table 1. Selected bond lengths and angles for the *trans* nitroso (OEP)Fe(AmphNO) moiety: Fe1–N5 = 1.8227(17) Å, N5–O1 = 1.284(2) [1.307(4)] Å, Fe(1)–N(por) = 1.9828(15)–2.0019(14) Å, ∠Fe1–N5–O1 = 121.96(14) [113.7(4)]°. Data for the minor disordered AmphNO component are shown in brackets. (B) Molecular structure of (TPP)Co(AmphNHOH): Co(1)–N(por) = 1.9742(18)–1.9859(18) Å. The two H atoms of the –NHOH moiety were located in the difference electron density map, and the H-bond between the porphyrin N4 atom and the NOH proton (H2) is represented by a dashed line (2.32 Å).

The identity of the hydroxylamine –NHOH moiety was clearly distinguishable from that of the *trans* –NO moiety based on the following: (i) the two H atoms of the –NHOH moiety were located in the difference electron density map and their positions refined independently, (ii) the Fe–NHOH (Fe–N6) bond is significantly longer than that for the *trans* axial Fe–N(nitroso) (Fe–

N5) bond and is close to the 2.028(2)–2.100(2) Å range [34, 35] determined in other porphyrin Fe-amine type complexes, and (iii) the N–O bond of the hydroxylamine moiety (1.432(2) Å) is significantly longer than the *trans* nitroso bond.

Unexpectedly, the hydroxy H-atom of the –NHOH moiety in the structure was found to form an internal H-bond with the porphyrin N4 (Figure 4A) with a H-bond N4···H3 distance of 2.19(3) Å. Interestingly, the N4 atom is also displaced from the porphyrin 24-atom mean plane by 0.087 Å in the direction of the H-bond. *To the best of our knowledge, such an internal H-bond from an axial ligand to a porphyrin N-atom has not been previously reported in metalloporphyrin structural chemistry.*

Table 1. Selected bond lengths (in Å) and angles (in °) for the ordered Fe–AmphNHOH and Co–AmphNHOH moieties in the Fe and Co complexes shown in Figure 4.[a]

	Fe	Co[c]	
AmphNHOH			
Fe1–N6	2.1405(17)	Co–N5	2.191(2)
N6–O2	1.432(2)	N5–O1	1.452(2)
N6–C54	1.488(3)	N5–C45	1.477(3)
Fe1–N6–O2	116.53(11)	Co1–N5–O1	114.99(13)
Fe1–N6–C54	124.30(13)	Co1–N5–C45	122.61(16)
C54–N6–O2	108.20(15)	C45–N5–O1	108.64(17)

[a] Data for the *trans* axial AmphNO ligand for Fe is shown in the caption for Figure 4, as are the Fe–N(por) and Co–N(por) distances.

This study was extended to cobalt to determine if the Co(III) center (isoelectronic with Fe(II)) could also assist in the net formal oxidation of the AmphNHOH ligand to the nitroso AmphNO

derivative during the binding events. In the case of Co, only the five-coordinate (TPP)Co(AmphNHOH) product was obtained (eq. 3; ~55% yield). The conversion of Co(III) to Co(II) was evident from the UV-vis monitoring of the reaction (Fig. S4)

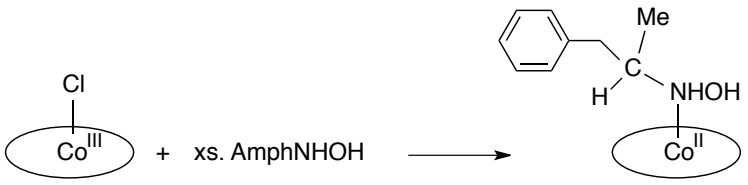

(3)

The molecular structure of the five-coordinate (TPP)Co(AmphNHOH) product is shown in Figure 4B. Selected geometrical data are presented in the caption and in Table 1. As with the Fe analog shown in Figure 4A, the H atoms of the –NHOH moiety of the axial ligand were located in the difference electron density map, and the crystal structure revealed a similar internal H-bonding feature involving the bound –NHOH group. This observed internal H-bond was also associated with an apical displacement of the porphyrin N4 atom (by +0.17 Å) from the 24-atom mean porphyrin plane) towards the H-bond. The Co atom was apically displaced by +0.13 Å from the porphyrin plane towards the AmphNHOH ligand [36].

In this Co case, we did not obtain the nitroso product (TPP)Co(AmphNO) under our reaction conditions, implying that the five-coordinate hydroxylamine (TPP)Co(AmphNHOH) product was kinetically more stable than the related Fe analogues.

2.1 Computational Insights

We employed DFT calculations on the isolated low-spin (TPP)Fe(AmphNHOH)(AmphNO) molecule to determine if the observed internal H-bond between the bound AmphNHOH group and a porphyrin N-atom was an intrinsic structural feature and not due to artifacts of crystallization or crystal packing effects.

Geometry optimization: Geometry optimization was performed using the ωB97X-D functional [37] and the LANL2DZ effective core potential (for Fe) [38] and 6-31+G* basis set (for the non-Fe atoms) [39, 40]. The calculated optimized geometry was in excellent agreement with the experimental X-ray structure, with an overall all-atom RMSD of 0.2443 Å; the largest deviations were in the peripheral porphyrin substituents (Figure 5).

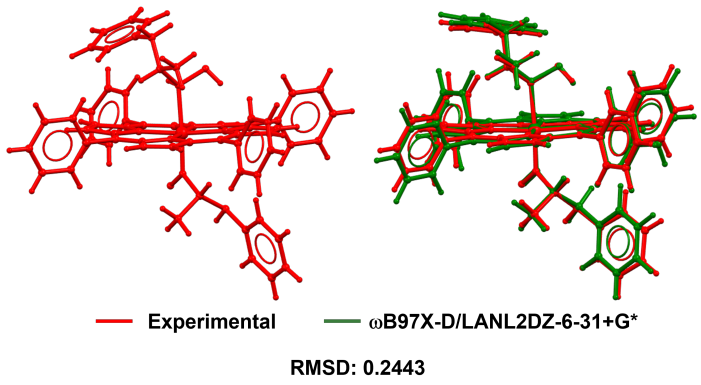

Fig. 5. Superposition of the experimental and calculated geometry-optimized structures of (TPP)Fe(AmphNHOH)(AmphNO).

Importantly, the calculated geometry-optimized structure also displayed the presence of the unique internal H-bond between the hydroxylamine –OH group and a porphyrin N-atom, with a (por)N···H(O) distance of 1.9718 Å which is in very good agreement with the experimental 2.19(3) Å. The apical displacement of the porphyrin N-atom (relative to the 24-atom porphyrin plane) involved in the internal H-bond was also reproduced quite well from the calculations (Table S3).

The related geometry optimization of the five-coordinate cobalt complex (TPP)Co(AmphNHOH) also generated a structure that was in excellent agreement with the experimental X-ray crystal structure, with an all-atom RMSD of 0.138 Å (Figure S5). The unique internal H-bond feature was also reproduced, with a (por)N···H(O) distance of 2.3386 Å in excellent agreement with the experimental distance of 2.32(3) Å.

2.2 Probing the Internal H-bond Preference by Scanning the Potential Energy Surface (PES)

To determine if other hydroxylamine Fe–NO*H* orientations were local minima on the potential energy surface (PES), we calculated the PES of the model ferrous complex (porphine)Fe(AmphNHOH)(NH_3) in the gas phase, where the experimental porphyrin macrocycle TPP was replaced by the unsubstituted porphine macrocycle, and the *trans* nitroso AmphNO ligand in the experimental structure was replaced with a simple N-donor ligand NH_3. The geometry scan was carried out by varying the hydroxylamine τC–N–O–H torsion angle; specifically, keeping the C–N–O fragment static and rotating the N–O–H bond (i.e., changing the H-atom positions) in sequential 10° increments over the full 360° range. The resulting geometries were reoptimized with the torsional angle constrained at each value and the single-point energies calculated. The AmphNHOH ligand in both the complex and in the free unbound state displayed τC–N–O–H torsion angle-dependent energy changes.

The PES scan for free unbound AmphNHOH is shown in Figure 6A. The global energy minimum occurs when the τC–N–O–H torsion angle is ca. 120°, placing the hydroxyl H-atom in a "down" position. A local energy minimum occurs when τC–N–O–H is ca. –70° (H-atom in an "up" position), and at 4.999 kcal/mol higher in energy than the global minimum.

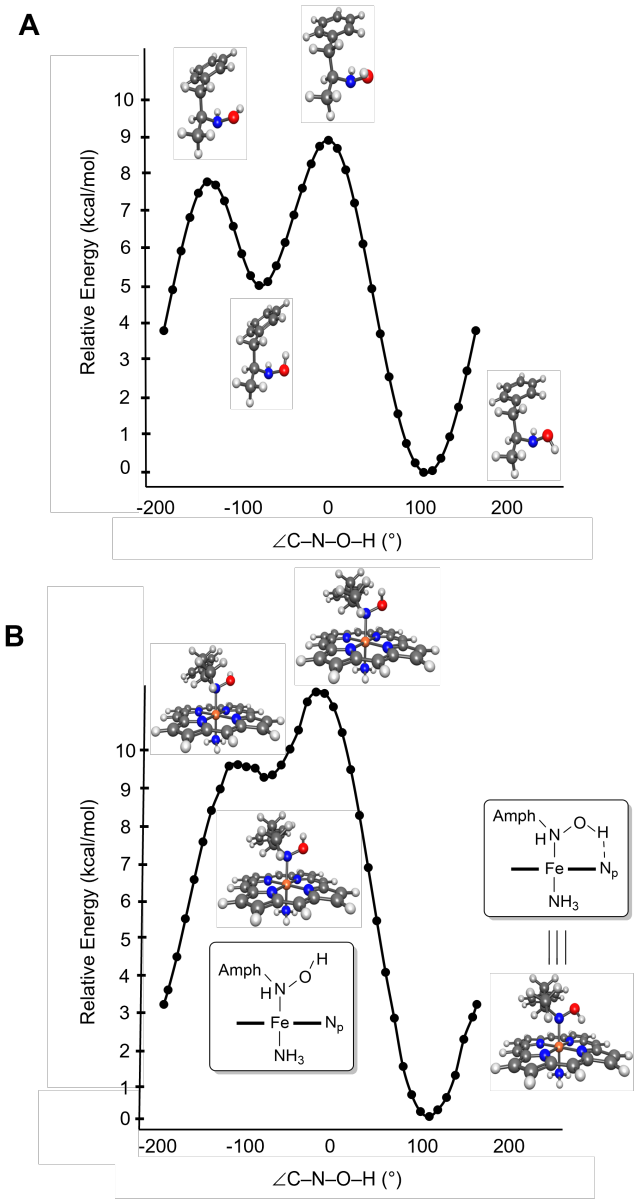

Fig. 6. Potential energy surfaces for (A) the free ligand AmphNHOH, (B) the truncated model (porphine)Fe^{II}(AmphNHOH)(NH_3) from ωB97X-D/6-31+G* calculations.

Figure 6B shows a similar global energy minimum for the (porphine)Fe(AmphNHOH)(NH_3) complex when the ∠C–N–O–H torsion angle is 125° and the hydroxyl H-atom is in a "down" position. In this bound AmphNHOH scenario, a local minimum is also observed when the ∠C–N–O–H torsion angle is –65°. In this (porphine)Fe(AmphNHOH)(NH_3) model, the energy

difference between the global and local minima is 9.277 kcal/mol. This suggests that binding of AmphNHOH to the (porphine)Fe system and associated internal H-bonding results in an additional 4.278 kcal/mol stabilization when referenced against the data for the free AmphNHOH ligand H-orientations in Figure 6A (i.e., 9.277–4.999 kcal/mol).

We also examined the related PES scan for the ferrous five-coordinate (porphine)Fe(AmphNHOH) to examine whether the presence of a sixth ligand alters the H-bond preference. The resulting data were similar to those obtained for the six-coordinate derivative (Figure S6). In this case, binding of AmpNHOH to the (por)Fe moiety resulted in an additional energy gain of the "down" conformation (i.e., with the internal H-bond) of 3.638 kcal/mol. These data suggest that the experimentally observed internal H-bond is an intrinsic structural feature and not due to crystal packing effects.

2.3 Natural Bond Orbital (NBO) Analysis

Having established the internal H-bond as an intrinsic geometrical feature of the (por)Fe(AmphNHOH)-containing system, we utilized second-order perturbative analysis [41] to elucidate the different molecular orbital interactions that contribute to the binding of the AmphNHOH ligand to the heme macrocycle. We performed these calculations using models based on the full experimental six-coordinate (TPP)Fe(AmphNHOH)(AmphNO) and five-coordinate (TPP)Co(AmphNHOH) structures. Selected data are presented in Table 2. As can be expected, the predominant interactions between the bound AmphNHOH ligands and the metal centers are from the lone pair (LP) donation from the liganded N-atom of AmphNHOH to the Fe (23.7 kcal/mol) and Co (7.7 kcal/mol) centers. Not surprisingly, the *trans* nitroso AmphNO ligand had a stronger interaction with the Fe center due to its π-acid nature.

Table 2. Natural Bond Orbital Analysis for (TPP)Fe(AmphNHOH)(AmphNO) and (TPP)Co(AmphNHOH) using ωB7X-D/ECP.

	Conformation	Donor NBO	Acceptor NBO	E (kcal/mol)
Iron	H "down"	π N8-C33	π* O3-H4	3.04
		π N10	*d** Fe	23.7
		π N9	*d** Fe (trans)	51.18
	H "up"	π N8-C33	π* O3- H4	-
		π N10	*d** Fe	19.5
		π N9	*d** Fe (trans)	42.15
Cobalt	H "down"	π N5-C17	π* O2-H3	1.36
		π N8	*d** Co	7.7
	H "up"	π N5-C17	π* O2-H3	-
		π N8	*d** Co	7.0

π = bonding orbital; located on a porphyrin pyrrole N=C fragment. π* = antibonding orbital; located on the hydroxyl OH group. Atom numbering refers to the calculated structures.

Intriguingly, the secondary interaction between the hydroxylamine AmphNHOH and (porphine)Fe moiety was further revealed in the calculations. We determined that a unique donor π orbital (located on the porphyrin/pyrrole N=C fragment) to an acceptor π* antibonding orbital of the hydroxyl group was present, and its interaction energy was calculated to be 3.04 kcal/mol (Table 2), accounting for ~11% of the heme–AmphNHOH interaction energy. The sketch of the primary molecular orbital interaction for the Fe case is shown in Figure 7, with relevant results displayed in Table 2 and visualized in Figure 8. Not surprisingly, this unique secondary H-bonding

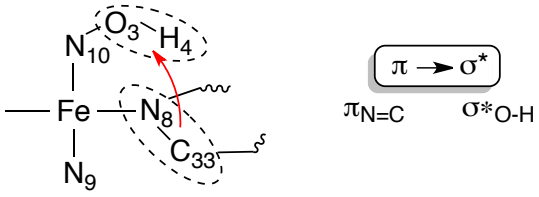

Fig. 7. Sketch of the porphyrin π-to-π*(O-H) interaction. Atom numbering refers to the calculated (TPP)Fe(AmphNHOH)(AmphNO) structure.

interaction was absent in the local energy minimum conformation that did not have the internal H-bond (i.e., the H "up" position; local minimum in Figure 6B).

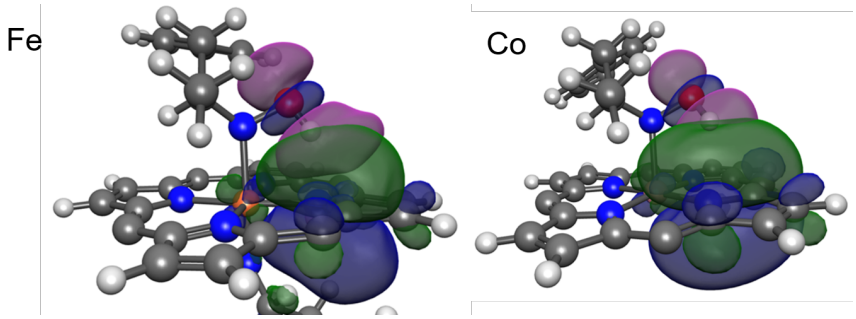

Fig. 8. NBO plot of (TPP)Fe(AmphNHOH)(AmphNO) and (TPP)Co(AmphNHOH) showing the interaction between the donor π N8-C33 → acceptor π* O3-H4 at the πB97X-D/LANL2DZ-6-31+G* level of theory.

The +3.04 kcal/mol interaction energy calculated for the full (TPP)Fe(AmphNHOH)(AmphNO) complex is in the same general range as the 4.278 kcal/mol derived from the PES scan for the (porphine)Fe(AmphNHOH)(NH_3) model. A similar π-to-π* interaction was determined for calculated (TPP)Co(AmphNHOH) but with a smaller interaction energy of 1.36 kcal/mol (Table 2 and Figure 8 (right)).

To examine the effect of this π-to-π* interaction on the O–H bond properties, we calculated the Mayer bond order of the free AmphNHOH ligand (in "H-down" position) and in the (TPP)Fe(AmphNHOH)(AmphNO) adduct. The results are shown in Figure 9 and Table S4, and

reveal that for the ligand N–H, N–C, and O–H bonds, they all increase in length and decrease in bond order upon binding, consistent with a weakening effect. Curiously, the N–O bond shows a decrease in both bond length and bond order upon coordination, and we are currently probing this further.

Overall, the NBO results are consistent with a unique heme-based activation of (by weakening) the hydroxyl O–H bond which would enhance reactivity to its nitroso derivative

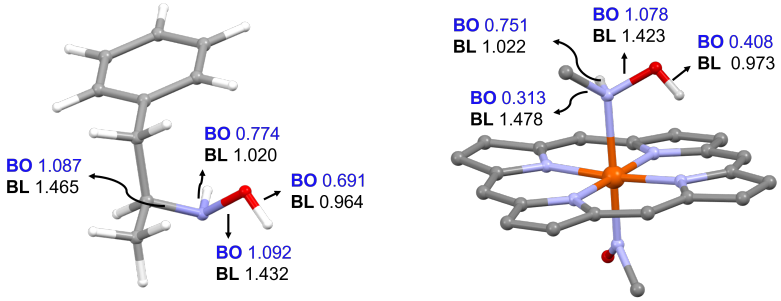

Fig. 9. Mayer bond order (BO) and bond length (BL) of the free ligand (AmphNHOH) and complex (TPP)Fe(AmphNHOH)(AmphNO). The Fe complex is truncated for clarity.

in the Fe case at ambient temperature. The lower □-to-□* interaction energy in the case of Co, and resulting lower O–H activation, helps explain the relative increased stability of the Co–AmphNHOH adduct as observed experimentally.

2.4 Extensions to the Parent Hydroxylamine NH_2OH

Although we have not succeeded in isolating and structurally characterizing an analogous synthetic heme–NH_2OH complex, we were interested in determining if the unique internal H-bond could be present in such compounds. We computationally probed both ferrous and ferric heme–NH_2OH models. Both ferrous and ferric hemes have been implicated in biological NH_2OH reactivity [19]. We also considered both the N-bound and O-bound linkage isomers of the Fe–NH_2OH derivatives in both low-spin and higher-spin (triplet, quintet) states, as we do not have

an isolated and/or structurally characterized example to build on. In both the ferric and ferrous (porphine)Fe(NH_2OH)(NH_3) models, the low-spin N-bound Fe–NH_2OH linkage isomers had the lowest energies. For example, the O-bound isomers were +10.15 kcal/mol and +10.53 kcal/mol higher in energy for the ferric and ferrous systems in their low-spin states, respectively (Table S5). We thus focused on the low-spin N-bound forms to probe the internal H-bond feature.

The potential energy scan for the low-spin ferric and ferrous N-bound NH_2OH models are shown in Figure 10; the analogous scan for the gas-phase free NH_2OH ligand is shown in

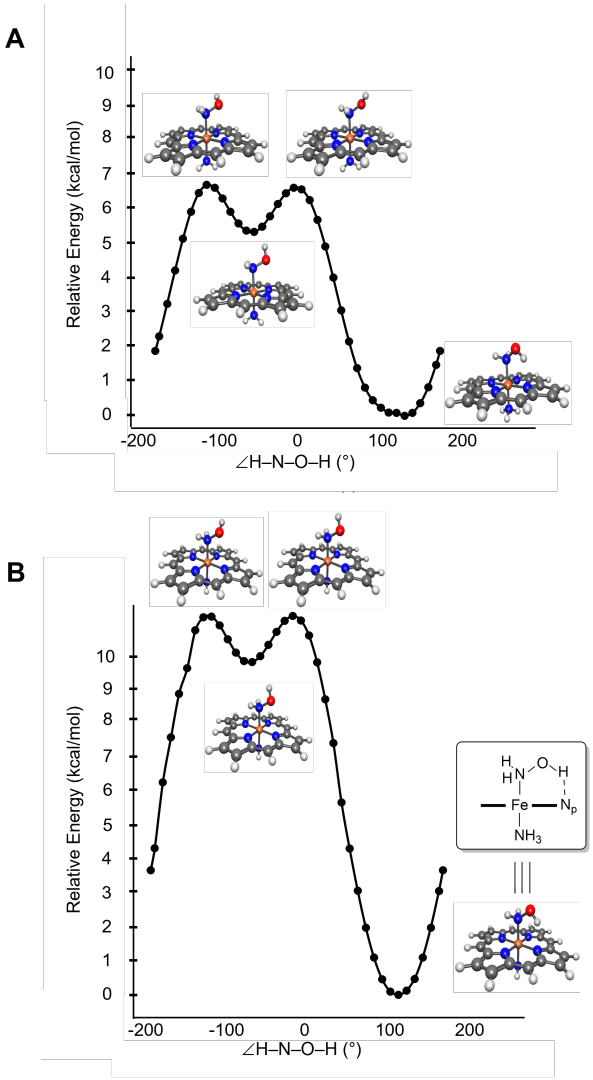

Fig. 10. Potential energy surfaces for (A) ferric (porphine)(Fe(NH_2OH)(NH_3) and (B) ferrous (porphine)Fe(NH_2OH)(NH_3) from □B97X-D/6-31+G* calculations.

Figure S7. Importantly, the geometry optimizations and subsequent potential energy surface scans reveal similar patterns of local and global energy minima as with the AmphNHOH analogues in Figure 6, and the presence of global minima that feature the presence of the internal H-bond. The energy difference between the local and global minima is calculated to be larger for the ferrous (9.99 kcal/mol) than for the ferric (5.37 kcal/mol), consistent with a view that the more electron-rich ferrous system would probably result in a larger π (porphyrin) to π^* (OH) donor-acceptor interaction.

NBO analysis of the ferrous (TPP)Fe(NH_2OH)(AmphNO) model showed a π (porphine) to π^* (O–H) interaction of 2.32 kcal/mol (Table S7), accounting for ~6% of the total Fe–NH_2OH interaction energy. This value is lower than the 3.04 kcal/mol calculated for the (TPP)Fe(AmphNHOH)(AmphNO) analogue (Table 2). The related interaction energy for the cobalt (TPP)Co(NH_2OH) model was calculated at 1.71 kcal/mol, which was higher than that for the (TPP)Co(AmphNHOH) model (1.36 kcal/mol; Table 2).

3. Epilogue

Our X-ray crystallographic determinations of (TPP)Fe(AmphNHOH)(AmphNO) and (TPP)Co(AmphNHOH) have revealed a previously unreported internal H-bond feature between the bound alkylhydroxylamines and porphyrin N-atoms. This feature was reproduced well by DFT calculations, and suggests that in the absence of competing protein active site distal pocket H-bonding interactions (e.g., in studies using heme models), that the presence (or absence) of such internal H-bonding should, at a minimum, be considered. Our extensions of the calculations to the parent NH_2OH ligand begs the question if such a feature could be present in other axial

four-atom Fe–X–Y–H moieties in hemes (left of Figure 11). One such scenario is H_2O_2 bound to heme (right of Figure 11). Indeed, our preliminary calculations with the model (porphine)Fe(H_2O_2)(NH_3) in both the ferrous and ferric low-spin forms reveal energy minima that correspond to the presence of the internal H-bond. The potential energy scans for the ferrous

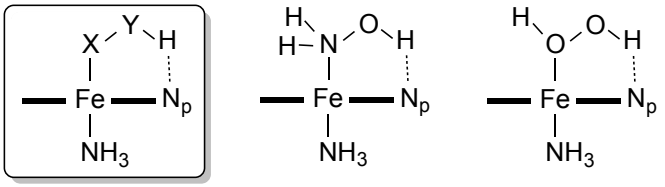

Fig. 11. Sketch of Fe–X–Y–H interactions as applied to Fe–NH_2OH and Fe–H_2O_2.

heme–H_2O_2 system reveal a single energy minimum coincident with the internal H-bond (Figure S8). In contrast, the scans for the ferric system revealed two degenerate energy minima with no distinct preference (ΔE <0.5 kcal/mol) for a geometrically positioned H-atom that engages in an internal H-bond (Figure S9). Importantly, we note that such internal H-bonds between a ferric heme-N atom and bound [42, 43] (or unbound [43, 44]) H_2O_2 have been proposed, based on QM/MM calculations, for some ground and transition state complexes that form during some cyt P450-enabled oxidations in the presence of substrates, although the contributions of the internal H-bonds to the overall reactivities were not significant in these cases.

In any event, our results for Fe–AmphNHOH (experimental and computational) and Fe–NH_2OH (computational) suggest that, indeed, such internal H-bonds for axial Fe–X–Y–H moieties may be more general than previously recognized and may serve to weaken the –NH*O*–*H* bond.

4. Experimental Section

Synthesis procedures were carried out anaerobically using Schlenk techniques and a glove box as described in the Supporting Information. Crystallographic data have been deposited with the CCDC (2104650-2104652) and can be obtained free of charge via www.ccdc.cam.ac.uk/data_request/cif. DFT calculations were performed using the Q-Chem software package [45] and the results visualized using IQmol. The Supporting Information contains experimental and computational details, and additional figures and tables.

5. Acknowledgements

This material is based upon work supported by (while GBR-A was serving at) the U.S. National Science Foundation (NSF; CHE-1900181). YS is supported by NSF Grant No. CHE-2102071. Any opinions, findings, and conclusions or recommendations expressed in this material are those of the authors and do not necessarily reflect the views of the NSF. We are grateful to the NSF MRI program (CHE-0130835) for funds to purchase the X-ray diffractometer.

6. Table of Abbreviations

AmphNHOH	*N*-hydroxyamphetamine
AmphNO	nitrosoamphetamine
DFT	density functional theory
ECP	effective core potential
Hb	hemoglobin
Imd	imidazole
i-Pr	isopropyl

LANL2DZ	Los Alamos National Laboratory 2 Double-Zeta
Mb	myoglobin
1-MeIm	1-methylimidazole
NBO	natural bond orbital
OEP	dianion of octaethylporphyrin
PES	potential energy surface
Por	dianion of a generic porphyrin
QM/MM	quantum mechanical/molecular mechanical
RMSD	root mean square deviation
TPP	dianion of tetraphenylporphyrin

7. References

[1] A.H. Beckett, P.M. Belanger, Metabolic incorporation of oxygen into primary and secondary aliphatic-amines and consequences in carbon-nitrogen bond-cleavage, J. Pharm. Pharmacol., 27 (1975) 547-552.

[2] J. Wright, A.K. Cho, J. Gal, The role of *N*-hydroxylamphetamine in the metabolic deamination of amphetamine, Life Sci., 20 (1977) 467-474.

[3] L. Li, T. Everhart, P. Jacob III, R. Jones, J. Mendelson, Stereoselectivity in the human metabolism of metamphetamine, Br. J. Clin. Pharmacol., 69 (2010) 187-192.

[4] V.M. Florence, E.W. Di Stefano, C.Y. Sum, A.K. Cho, The metabolism of (*R*)-(-)-amphetamine by rabbit liver microsomes: Initial products, Drug Metab. Disp., 10 (1982) 312-315.

[5] J.R. Cashman, Y.N. Xiong, L. Xu, A. Janowsky, *N*-Oxygenation of amphetamine and methamphetamine by the human flavin-containing monooxygenase (Form 3): Role in bioactivation and detoxification, J. Pharmacol. Exp. Ther., 288 (1999) 1251-1260.

[6] D. Mansuy, E. Rouer, C. Bacot, P. Gans, J.C. Chottard, J.P. Leroux, Interaction of aliphatic *N*-hydroxylamines with microsomal cytochrome P450: Nature of the different derived

complexes and inhibitory effects on monooxygenases activities, Biochem. Pharmacol., 27 (1978) 1229-1237.

[7] D. Mansuy, P. Beaune, J.C. Chottard, J.F. Bartoli, P. Gans, The nature of the "455 nm absorbing complex" formed during the cytochrome P450 dependent oxidative metabolism of amphetamine, Biochem. Pharmacol., 25 (1976) 609-612.

[8] J. Jonsson, B. Lindeke, On the formation of cytochrome P-450 product complexes during the metabolism of phenylalkylamines, Acta Pharm. Suec., 13 (1976) 313-320.

[9] M.R. Franklin, Complexes of metabolites of amphetamines with hepatic cytochrome P-450, Xenobiotica, 4 (1974) 133-142. *Chem. Abs.* 1**82**:118715h.

[10] S.M. Powell, L.M. Thomas, G.B. Richter-Addo, The nitrosoamphetamine metabolite is accommodated in the active site of human hemoglobin: Spectroscopy and crystal structure, J. Inorg. Biochem., 213 (2020) 111262.

[11] B. Wang, S.M. Powell, Y. Guan, N. Xu, L.M. Thomas, G.B. Richter-Addo, Nitrosoamphetamine binding to myoglobin and hemoglobin: Crystal structure of the H64A myoglobin-nitrosoamphetamine adduct, Nitric Oxide, 67 (2017) 26-29.

[12] A. Soler-Jofra, J. Perez, M.C.M. van Loosdrecht, Hydroxylamine and the nitrogen cycle: A review, Water Res, 190 (2021) 116723.

[13] A.A. Pacheco, J. McGarry, J. Kostera, A. Corona, Techniques for investigating hydroxylamine disproportionation by hydroxylamine oxidoreductases, Methods Enzymol., 486 (2011) 447-463.

[14] C. Ferousi, S.H. Majer, I.M. DiMucci, K.M. Lancaster, Biological and bioinspired inorganic N-N bond-forming reactions, Chem. Rev., 120 (2020) 5252-5307.

[15] R.E. Coleman, K.M. Lancaster, Heme P460: A (cross) link to nitric oxide, Acc. Chem. Res., 53 (2020) 2925-2935.

[16] P. Cedervall, A.B. Hooper, C.M. Wilmot, Structural studies of hydroxylamine oxidoreductase reveal a unique heme cofactor and a previously unidentified interaction partner, Biochemistry, 52 (2013) 6211-6218.

[17] M.A. Smith, S.H. Majer, A.C. Vilbert, K.M. Lancaster, Controlling a burn: Outer-sphere gating of hydroxylamine oxidation by a distal base in cytochrome P460, Chem. Sci., 10 (2019) 3756-3764.

[18] J. Kostera, J. McGarry, A.A. Pacheco, Enzymatic interconversion of ammonia and nitrite: the right tool for the job, Biochemistry, 49 (2010) 8546-8553.

[19] O. Einsle, A. Messerschmidt, R. Huber, P.M.H. Kroneck, F. Neese, Mechanism of the six-electron reduction of nitrite to ammonia by cytochrome *c* nitrite reductase, J. Am. Chem. Soc., 124 (2002) 11737-11745.

[20] A. Dietl, C. Ferousi, W.J. Maalcke, A. Menzel, S. de Vries, J.J. Keltjens, M.S. Jetten, B. Kartal, T.R. Barends, The inner workings of the hydrazine synthase multiprotein complex, Nature, 527 (2015) 394-397.

[21] S. Nakano, M. Takahashi, A. Sakamoto, H. Morikawa, K. Katayanagi, The reductive reaction mechanism of tobacco nitrite reductase derived from a combination of crystal structures and ultraviolet-visible microspectroscopy, Proteins: Struct., Func., Genet., 80 (2012) 2035-2045.

[22] K. Fukuyama, T. Okada, Structures of cyanide, nitric oxide and hydroxylamine complexes of *Arthromyces ramosus* peroxidase at 100 K refined to 1.3 angstrom resolution: Coordination geometries of the ligands to the haem iron, Acta Crystallogr D, 63 (2007) 472-477.

[23] D. Feng, M.D. Ryan, Electrochemistry of nitrite reductase model compounds. 3. Formation and characterization of a bis(hydroxylamine)(tetraphenylporphyrinato)iron(II) complex, Inorg. Chem., 26 (1987) 2480-2483.

[24] M.L. Fernandez, D.A. Estrin, S.E. Bari, Theoretical insight into the hydroxylamine oxidoreductase mechanism, J. Inorg. Biochem., 102 (2008) 1523-1530.

[25] A.A.A. Attia, R. Silaghi-Dumitrescu, Computational investigation of the initial two-electron, two-proton steps in the reaction mechanism of hydroxylamine oxidoreductase, J. Phys. Chem. B, 118 (2014) 12140-12145.

[26] A few small-molecule metal-NH_2OH adducts in coordination compounds have been characterized by X-ray crystallography (refs. 27-31).

[27] S. Matsukawa, S. Kuwata, Y. Ishii, M. Hidai, Coordination behaviour of (diaryl disulfide)-bridged dinuclear thiairidaindan cores: Ligand substitution by isocyanides, CO, hydrazines and hydroxylamine, and related reactions, J Chem Soc Dalton, (2002) 2737-2746.

[28] E. Chardon, G. Dahm, G. Guichard, S. Bellemin-Laponnaz, Exploring nitrogen ligand diversity in *trans*-*N*-heterocyclic carbene-amine platinum complexes: Synthesis, characterization, and application to fluorescence, Chem. Asian J., 8 (2013) 1232-1242.

[29] L.M. Engelhardt, P.W.G. Newman, C.L. Raston, A.H. White, Crystal structure of hexakis(hydroxylamine-*N*)nickel(II) sulphate, Aust. J. Chem., 27 (1974) 503-507.

[30] J.S. Southern, G.L. Hillhouse, A.L. Rheingold, Preparation of a nitroxyl (HN=O) complex of rhenium by selective oxidation of coordinated hydroxylamine, J. Am. Chem. Soc., 119 (1997) 12406-12407.

[31] H.G. Zheng, W.H. Leung, J.L.C. Chim, W. Lai, C.H. Lam, I.D. Williams, W.T. Wong, Heterobimetallic μ-nitrido complexes containing ruthenium(II) dithiocarbamate, Inorg Chim Acta, 306 (2000) 184-192.

[32] D. Mansuy, P. Battioni, J.-C. Chottard, C. Riche, A. Chiaroni, Nitrosoalkane complexes of iron-porphyrins: analogy between the bonding properties of nitrosoalkanes and dioxygen, J. Am. Chem. Soc., 105 (1983) 455-463.

[33] C.D. Sohl, J. Lee, S.S. Alguindigue, M.A. Khan, G.B. Richter-Addo, Synthesis and solid-state molecular structures of nitrosoalkane complexes of iron porphyrins containing methanol, pyridine, and 1-methylimidazole ligands, J. Inorg. Biochem., 98 (2004) 1238-1246.

[34] O.Q. Munro, P.S. Madlala, R.A.F. Warby, T.B. Seda, G. Hearne, Structural, conformational, and spectroscopic studies of primary amine complexes of iron(II) porphyrins, Inorg. Chem., 38 (1999) 4724-4736.

[35] E.G. Abucayon, J.-M. Chu, M. Ayala, R.L. Khade, Y. Zhang, G.B. Richter-Addo, Insight into the preferential N-binding *versus* O-binding of nitrosoarenes to ferrous and ferric heme centers, Dalton Trans., 50 (2021) 3487-3498.

[36] An unresolved difference peak of 1.194e/Å^3 was located ~1.79 Å from C18; two possibilities considered were (i) a Cl atom coordinated to C18 (unlikely) or a whole molecule disorder where this is the Co atom of the disordered group.

[37] J.-D. Chai, M. Head-Gordon, Long-range corrected hybrid density functionals with damped atom-atom disperson corrections, Phys. Chem. Chem. Phys., 10 (2008) 6615-6620.

[38] P.J. Hay, W.R. Wadt, Ab initio effective core potentials for molecular calculations. Potentials for main group elements Na to Bi, J. Chem. Phys., 82 (1985) 299-310.

[39] W.J. Hehre, R. Ditchfield, J.A. Pople, Self-consistent molecular orbital methods. XII. Further extensions to Gaussian-type basis sets for use in molecular orbital studies of organic molecules, J. Chem. Phys., 56 (1972) 2257-2261.

[40] P.C. Hariharan, J.A. Pople, The influence of polarization functions on molecular orbital hydrogenation energies, Theor. Chim. Acta, 28 (1973) 213-222.

[41] A.E. Reed, L.A. Curtiss, F. Weinhold, Intermolecular interactions from a natural bond orbital, donor-acceptor viewpoint, Chem. Rev., 88 (1988) 899-926.

[42] B. Wang, C. Li, K.D. Dubey, S. Shaik, Quantum mechanical/molecular mechanical calculated reactivity networks reveal how cytochrome P450cam and its T252A mutant select their oxidation pathway, J. Am. Chem. Soc., 137 (2015) 7379-7390 (Fig. S20).

[43] M. Altarsha, T. Benighaus, D. Kumar, W. Thiel, How is the reactivity of cytochrome P450cam affected by Thr252X mutation? A QM/MM study for X = serine, valine, alanine, glycine, J. Am. Chem. Soc., 131 (2009) 4755-4763 (Figs. S5, S8-9, S18, S22).

[44] B. Wang, C. Li, K.-B. Cho, W. Nam, S. Shaik, The $Fe^{III}(H_2O_2)$ complex as a highly efficient oxidant in sulfoxidation reactions: Revival of an underrated oxidant in cytochrome P450, J. Chem. Theory Comput., 9 (2013) 2519-2525 (Fig. S20).

[45] E.Epifanovsky et al., Software for the frontiers of quantum chemistry: An overview of developments in the Q-Chem 5 Package, J. Chem. Phys., 155 (2021) 084801-084859.

Graphical Abstract

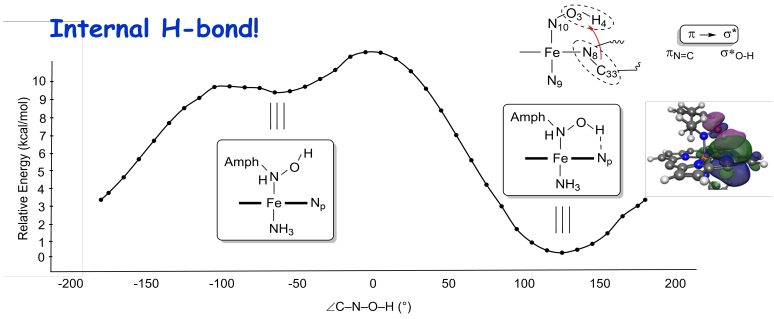

Synopsis for Graphical Abstract:

Crystal structures of *N*-hydroxyamphetamine (AmphNHOH) in complex with Fe and Co heme models demonstrate an internal H-bond interaction between the AmphNH*O–H* group and a porphyrin N-atom. Calculations and natural bond orbital analyses reveal a donor π ($por_{N=C}$) to acceptor σ^* (O–H) interaction that weakens the AmphNHO–H bond.

Supporting Information

Interactions of N-hydroxylamine with an iron porphyrin: A unique intramolecular H-bond probed by DFT calculations

Ye Guan, Jennifer Londoño-Salazar, Zheng Pei, Douglas R. Powell, Yihan Shao* and George B. Richter-Addo*

Price Family Foundation of Structural Biology and Department of Chemistry and Biochemistry, University of Oklahoma, Norman, OK 73019

CONTENTS

FIGURES

TABLES

Computed optimized structures (Cartesian coordinates).

Experimental

General: The reactions were performed under anaerobic conditions under an atmosphere of nitrogen using standard Schlenk techniques and/or in an Innovative Technology Labmaster 100 Dry Box unless stated otherwise. Nitroethane (99.5%), sodium borohydride (98.5%), *N*-butylamine (99%), benzaldehyde (99%), BH_3·THF (1M in THF) were purchased from Sigma-Aldrich. Anhydrous ethanol (ACS grade; Pharmco-AAPER), sodium bicarbonate (EM Science), anhydrous magnesium sulfate (97%; Mallinckrodt), hydrochloric acid (37%; EMD Chemicals), anhydrous ether (99.9%; J. T. Baker), and (TPP)Co (TPP = tetraphenylporphyrin dianion; Midcentury Chemicals) were purchased from commercial suppliers. (TPP)FeCl and (TPP)CoCl were prepared following standard literature methods. Solvents used for the reactions (THF, CH_2Cl_2, hexane) were obtained from an Innovative Technology Pure Solv 400-5-MD Solvent Purification system under an atmosphere of nitrogen. A Bio-Rad FT-155 FTIR spectrometer was used to record the infrared spectra. Proton NMR spectra were recorded on Varian Mercury VX 300 MHz or VXR-S 400 MHz spectrometers for room temperature and low temperature experiments, respectively, and the signals were referenced to the chloroform-*d* solvent employed.

Preparation of 1-phenyl-2-nitropropene. This compound was prepared following a literature procedure[1] with a slight modification. To a mixture of nitroethane (1.4 mL, 0.02 mol) and benzaldehyde (2.1 mL, 0.02 mol) in anhydrous ethanol (5 mL) was added *n*-butylamine (0.1 mL, 0.001 mol). The mixture was refluxed for 8 h and then cooled to room temperature, and cooled further on ice with stirring. This resulted in the formation of a pale yellow crystalline material. The crystalline material was washed with water and methanol to remove the orange colored impurities. The product (~60% crude yield) was identified by its characteristic ^{1}H NMR spectrum.[2] ^{1}H NMR (δ, $CDCl_3$): 8.10 (s, 1H, CH), 7.44 (m, 5H, C_6H_5), 2.42 (s, 3H, CH_3).

Preparation of N-hydroxyamphetamine.[3] A Schlenk tube was cooled to 0 °C on ice, and to it was added BH_3·THF (2.65 mL, 2.7 mmol) via syringe. In a separate Schlenk tube, 1-phenyl-2-nitropropene (0.45 g, 2.7 mmol) was dissolved in THF (9.5 mL). The solution of 1-phenyl-2-nitropropene was slowly added to the BH_3·THF solution (still cooled with an ice bath). After addition was complete, the ice bath was removed, and a catalytic amount of $NaBH_4$ (~40 mg) was added into the mixture. The solution was kept stirring until the yellow color of the starting material turned clear. Iced water (40 mL) and HCl (10%; 5.5 mL) were then added to the mixture. The mixture was refluxed at 65 °C for 2 h, and then allowed to cool to room temperature. The organic-soluble compounds were extracted with ether and discarded. Sodium carbonate was added to remaining aqueous fraction to neutralize the solution. Solid NaCl was the added to the solution until saturation. The products were extracted with ether in three cycles. Anhydrous $MgSO_4$ was used to dry the extracts overnight. The mixture was filtered and the solvent removed from the filtrate to give the white powdery *N*-hydroxyamphetamine product (~45% yield by weight). In our hands, the *N*-hydroxyamphetamine product can be kept at –20 °C in a glove box for several weeks without showing signs of decomposition. However, it will gradually decompose to a yellow liquid if kept at room temperature. ^{1}H NMR ($CDCl_3$): 7.19-7.32 (m, 5H, phenyl group), 3.21 (m, 1H, CH), 2.65 (dd, 1H, CH_2), 2.85 (dd, 1H, CH_2). The peaks for the protons of the –NHOH group were not observed.

Preparation of (OEP)Fe(AmphNO)(1-MeIm). Excess *N*-hydroxyamphetamine (0.037 g, 0.2 mmol) was added to a stirred solution of (OEP)FeCl (0.037 g, 0.06 mmol) in CH_2Cl_2 (5 mL). The color of the solution changed from brown red to black purple during a 6 h period. 1-MeIm (0.02 mL, 0.25 mmol) was added to the solution and the mixture was stirred overnight. The solution was dried in vacuo and redissolved in a CH_2Cl_2/hexane (1:1) mixture. 1-MeIm (0.01 mL, 0.125 mmol) was added to this solution. Purple plate-shaped crystals formed during slow evaporation of the mixture in the dry box at room temperature and were isolated in 58% yield. IR (KBr, cm^{-1}): υ_{NO} = 1419 m; also 1559 m, 1507 m,

1457 s, 1374 w, 1337 w, 1251 m, 1224 m, 1143 m, 1107 s, 1085 w, 1018 s, 955 s, 829 m, 745 s, 700 s. ^{1}H NMR ($CDCl_3$, δ ppm): 9.73 (s, 4H, *meso*-H of OEP), 3.93 (q, 16H, CH_2CH_3 of OEP), 1.82 (t, 24H, CH_2CH_3 of OEP), 6.75–7.00 (m, *p,m*-H of C_6H_5), 5.78 (d, 2H, *o*-H of C_6H_5), –0.58 (m, 1H, CH_2), –1.58 (app m, 1H, CH), –1.74 (d, 1H, CH_2), –2.52 (d, 3H, CH_3). The peaks of 1-MeIm were not observed at room temperature, but could be observed in the NMR spectrum at lower -40 °C. ^{1}H NMR ($CDCl_3$, –40 °C): 4.55 (s, 1H of 1-MeIm), 1.90 (s, overlapping with CH_2CH_3 of OEP, CH_3 of 1-MeIm), 0.95 (s, 1H of 1-MeIm), 0.6 (s, 1H of 1-MeIm).

Preparation of (TPP)Fe(AmphNHOH)(AmphNO). Excess *N*-hydroxyamphetamine (0.015 g, 0.1 mmol) was added into to a stirred solution of (TPP)FeCl (0.015 g, 0.02 mmol) in CH_2Cl_2 (5 mL) and left to stir overnight (~12 h). The product was taken to dryness in vacuo. The residue was re-dissolved in CH_2Cl_2 (1 mL), and hexane (~6 mL) was then careful layered on the top of the CH_2Cl_2 solution. Black block-shaped crystals formed at the bottom of the solution over a 2-week period. The crystals were identified as the air-sensitive (TPP)Fe(AmphNHOH)(AmphNO) product (~40% isolated yield) by X-ray crystallography. IR (KBr, cm^{-1}): υ_{NO} = 1435 m; also 1599 s, 1538 w, 1494 s, 1453 s, 1349 m, 1303 m, 1259 m, 1204 w, 1177 w, 1073 m, 1002 s, 796 m, 744 s, 700 s.

Preparation of (TPP)Co(AmphNHOH). Excess *N*-hydroxyamphetamine (0.03 g, 0.2 mmol) was added into a stirred CH_2Cl_2 solution of (TPP)CoCl (0.015 g, 0.02 mmol), and the reaction left to stir overnight, during which time the color of the solution changed from red-purple to an orange color. The solution was taken to dryness in vacuo and the residue was washed with methanol. The residue was redissolved in CH_2Cl_2, and hexane was added (2:1 ratio). Slow evaporation of this CH_2Cl_2/hexane (2:1) solution in a glove box resulted in the formation of cubic brown crystals within 1 week. The crystals were isolated and the air-sensitive product identified as (TPP)Co(AmphNHOH) (~55% isolated yield; λ_{max} 411 nm) by X-ray crystallography.

Crystallographic details

Intensity data for the compounds were collected using a D8 diffractometer with a Bruker APEX ccd area detector[4-5] and a sealed-tube Mo Kα source (λ = 0.71073 Å). The samples were cooled to 100(2) K. The structure was solved by direct methods and refined by full-matrix least-squares methods on F^2.[6-7]

(i) *(OEP)Fe(AmphNO)(1-MeIm)* (CCDC 2104652). A purple, plate-shaped crystal of dimensions 0.120 x 0.290 x 0.380 mm was selected for structural analysis. The intensity data were truncated to 0.87 Å because data in higher resolution shells all had <I/σ(I)> of <2. Cell parameters were determined from a least-squares fit of 4940 peaks in the range 2.21 < θ < 21.69°. A total of 46847 data were measured in the range 1.448 < θ < 24.108° using ϕ and ω oscillation frames. The data were corrected for absorption by the semi-empirical from equivalents method[8] giving minimum and maximum transmission factors of 0.865 and 0.954. The data were merged to form a set of 6872 independent data with R(int) = 0.1436 and a coverage of 100.0%.

The monoclinic space group $P2_1/n$ was determined by systematic absences and statistical tests and verified by subsequent refinement. The positions of hydrogens bonded to carbons were initially determined by geometry and were refined using a riding model. Non-hydrogen atoms were refined with anisotropic displacement parameters. Hydrogen atom displacement parameters were set to 1.2 (1.5 for methyl) times the isotropic equivalent displacement parameters of the bonded atoms. A total of 652 parameters were refined against 674 restraints and 6872 data to give wR(F^2) = 0.2554 and S = 1.008 for weights of w = 1/[$\sigma^2(F^2)$ + (0.1060 P)^2 + 20.40000 P], where P = [F_o^2 + 2F_c^2]/3. The final R(F) was 0.0934 for the 4403 observed, [F > 4σ(F)], data. The largest shift/s.u. was 0.002 in the final refinement cycle. The final difference map had maxima and minima of 0.903 and –0.833 e/Å^3, respectively.

Note on the disorder: There were three different areas of disorder in the structure. The occupancies of atoms O1 and C41–49 of the AmphNO ligand refined to 0.816(5) and 0.184(5) for the unprimed and primed atoms, respectively. The occupancies of ethyl atoms C29–30 of the OEP macrocycle refined to 0.756(12) and 0.244(12) for the unprimed and primed atoms, respectively. The occupancies of ethyl atoms C21–C22 of the OEP macrocycle refined to 0.677(11) and 0.323(11) for the unprimed and primed atoms, respectively. Restraints on the positional and displacement parameters of the disordered atoms were required.

(ii) *(TPP)Fe(AmphNHOH)(AmphNO)* (CCDC 2104650). A purple, plate-shaped crystal of dimensions 0.050 x 0.320 x 0.520 mm was selected for structural analysis. Cell parameters were determined from a least-squares fit of 9892 peaks in the range 2.33 < θ < 28.33°. A total of 74573 data were measured in the range 1.490 < θ < 28.337° using ϕ and ω oscillation frames. The data were corrected for absorption by the semi-empirical from equivalents method[8] giving minimum and maximum transmission factors of 0.686 and 0.746. The data were merged to form a set of 12081 independent data with R(int) = 0.0424 and a coverage of 100.0%.

The monoclinic space group $P2_1/c$ was determined by systematic absences and statistical tests and verified by subsequent refinement. The positions of hydrogens bonded to carbons were initially determined by geometry and were refined using a riding model. H-atoms bonded to N6 and O2 of the ordered –NHOH moiety were located on a difference map, and their positions were refined independently. Non-hydrogen atoms were refined with anisotropic displacement parameters. Hydrogen atom displacement parameters were set to 1.2 (1.5 for methyl) times the isotropic equivalent displacement parameters of the bonded atoms. A total of 737 parameters were refined against 410 restraints and 12081 data to give wR(F^2) = 0.1335 and S = 1.008 for weights of w = 1/[$\sigma^2(F^2)$ + (0.0670 P)^2 +

4.1000 P], where P = [F_o^2 + 2F_c^2]/3. The final R(F) was 0.0459 for the 9498 observed, [$F > 4\sigma(F)$], data. The largest shift/s.u. was 0.001 in the final refinement cycle. The final difference map had maxima and minima of 0.527 and –0.554 e/Å^3, respectively.

Note on the disorder: The *trans* axial AmphNO ligand was disordered. The occupancies of atoms O1 and C45-C53 refined to 0.824(2) and 0.176(2) for the unprimed and primed atoms, respectively. Restraints on the positional and displacement parameters of the disordered atoms were required.

(iii) *(TPP)Co(AmphNHOH)* (CCDC 2104651). A black, block-shaped crystal of dimensions 0.18 x 0.25 x 0.48 mm was selected for structural analysis. Cell parameters were determined from a least-squares fit of 5467 peaks in the range 2.51 < θ < 28.25°. A total of 26724 data were measured in the range 1.480 < θ < 26.372° using ϕ and ω oscillation frames. The data were corrected for absorption by the semi-empirical from equivalents method[8] giving minimum and maximum transmission factors of 0.803 and 0.919. The data were merged to form a set of 8145 independent data with R(int) = 0.0245 and a coverage of 99.9%.

The triclinic space group *P*-1 was determined by statistical tests and verified by subsequent refinement. The positions of hydrogens bonded to carbons were initially determined by geometry and were refined using a riding model. H-atoms bonded to O1 and N5 were located on a difference map, and their positions were refined independently. Non-hydrogen atoms were refined with anisotropic displacement parameters. Hydrogen atom displacement parameters were set to 1.2 (1.5 for methyl) times the isotropic equivalent displacement parameters of the bonded atoms. A total of 547 parameters were refined against 36 restraints and 8145 data to give wR(F^2) = 0.1376 and S = 1.009 for weights of w = 1/[$\sigma^2(F^2)$ + (0.0838 P)^2 + 1.4000 P], where P = [F_o^2 + 2F_c^2]/3. The final R(F) was 0.0473 for the 6879 observed, [$F > 4\sigma(F)$], data. The largest shift/s.u. was 0.001 in the final refinement cycle. The final difference map had maxima and minima of 1.194 and –0.295 e/Å^3, respectively.

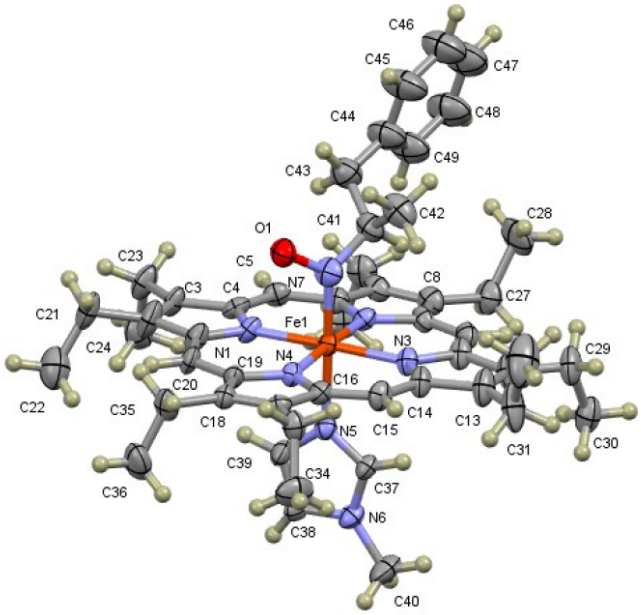

Figure S1. X-ray crystal structure of (OEP)Fe^{II}(AmphNO)(1-MeIm) with atom numbering, showing only the major (82%) disordered AmphNO ligand with N7 ordered. Thermal ellipsoids are drawn at 50%.

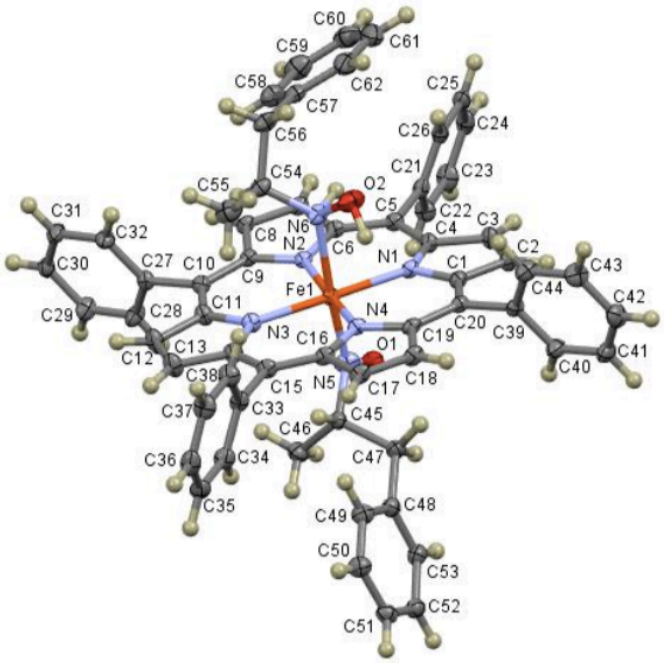

Figure S2. X-ray crystal structure of (TPP)Fe^{II}(AmphNHOH)(AmphNO) with atom numbering. Thermal ellipsoids are drawn at 50%.

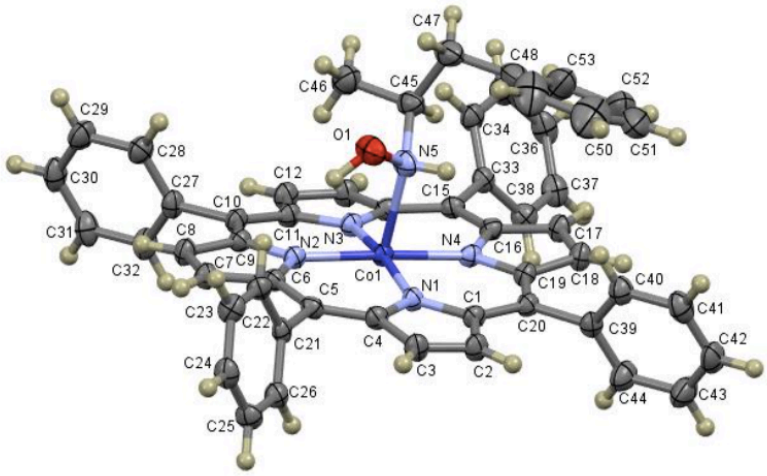

Figure S3. X-ray crystal structure of (TPP)Co^{II}(AmphNHOH) with atom numbering.

Table S1. Crystallographic data collection and refinement parameters

Complex	(OEP)Fe(AmphNO)(1-MeIm)	(TPP)Fe(AmphNHOH)(AmphNO)	(TPP)Co(AmphNHOH)
Empirical formula (f.w.)	$C_{49}H_{61}FeN_7O$ (819.89)	$C_{62}H_{52}FeN_6O_2$ (968.94)	$C_{53}H_{41}CoN_5O$ (822.84)
Crystal system, space group	monoclinic, $P2_1/n$	monoclinic, $P2_1/c$	triclinic, $P\ \bar{1}$
Unit cell dimensions			
a (Å)	10.3034(19)	12.9732(11)	12.0602(8)
b (Å)	17.208(3)	18.9168(17)	12.7994(9)
c (Å)	24.475(4)	20.2256(18)	14.9820(10)
α (°)	90	90	104.714(2)
β (°)	94.169(4)	102.3473(14)	101.437(2)
γ (°)	90	90	110.087(2)
Volume (Å^3)	4328.0(13)	4848.8(7)	1994.3(2)
Z, *Z*'	4, 1	4, 1	2, 1
Density (calc.) Mg/m^3	1.258	1.327	1.370
F(000)	1752	2032	858
Absorption coeff. (mm^{-1})	0.394	0.364	0.479
Max. and min. transm.	0.954 and 0.865	0.746 and 0.686	0.919 and 0.803
Theta range for data collection (°)	1.448 to 24.108	1.490 to 28.337	1.480 to 26.372
Reflections collected	46847	74573	26724
Independent reflections	6872 [R(int) = 0.1436]	12081 [R(int) = 0.0424]	8145 [R(int) = 0.0245]
Data/restraints/parameters	6872 / 674 / 652	12081 / 410 / 737	8145/ 36 / 547
wR(*F*2 all data) [a]	*wR2* = 0.2554	*wR*2 = 0.1335	*wR*2 = 0.1376
R(*F* obsd data) [b]	*R1* = 0.0934	*R*1 = 0.0459	*R*1 = 0.0473
Goodness-of-fit on F^2	1.008	1.008	1.009
Observed data [I > 2σ(I)]	4403	9498	6879
Largest and mean shift / s.u.	0.002 and 0.000	0.001 and 0.000	0.001 and 0.000
Largest diff. peak and hole (e/Å^3)	0.903 and –0.833	0.527 and –0.554	1.194 and –0.295

a wR2 = $\{ \Sigma [w(F_o^2 - F_c^2)^2] / \Sigma [w(F_o^2)^2] \}^{1/2}$ [b] $R1 = \Sigma ||F_o| - |F_c|| / \Sigma |F_o|$

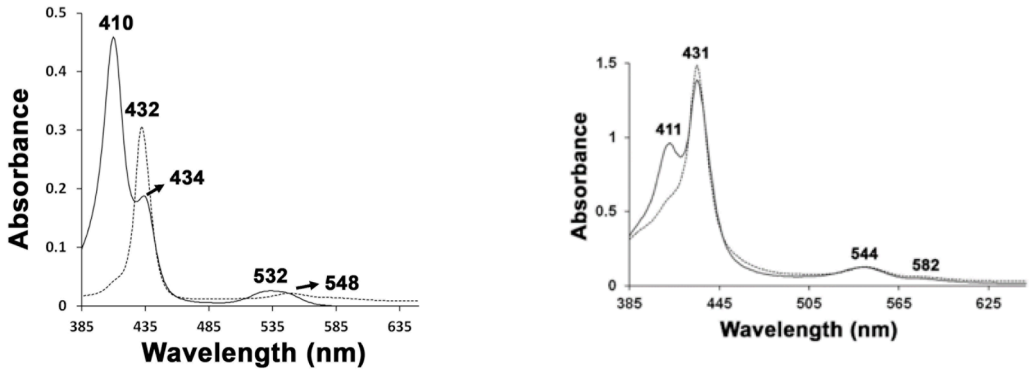

Figure S4. *Left:* UV-vis spectra of the reaction between (TPP)CoCl and AmphNHOH in CH_2Cl_2 in air. *Solid line*: spectrum of the initial product solution. *Dashed line*: after addition of 1-MeIm and overnight stirring. *Right*: *Solid line:* The UV-vis spectrum of a dissolved crystal of (TPP)Co(AmphNHOH) in CH_2Cl_2 in air. *Dashed line:* After leaving the solution in air for ~8 h.

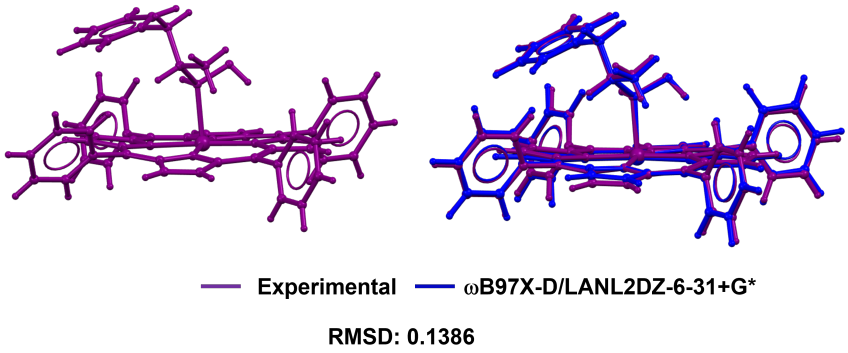

Figure S5. Superposition of the experimental and calculated geometry-optimized structures of (TPP)Co^{II}(AmphNHOH).

Computational Methodology and Results

All quantum mechanical (QM) electronic ground-state calculations were performed using the density functional theory (DFT) method.[9-10] Version 5.0 of the Q-Chem software package[11] was used as well as IQmol as visualization package. Molecular geometry optimization and energy studies were carried out using the ωB97X-D[12] functional and LANL2DZ effective core potential[13] (for Fe) and 6-31+G* basis set[14-15] (for the non-Fe atoms).The funtional/basis set that best reproduced the experimental values from the X-ray structures was ωB97X-D as functional and LANL2DZ/6-31+G* as basis set, giving a good balance between reliability and computational speed. Once the ground-state geometry was obtained, the PES-SCAN, NBO analysis and vibrational frequencies were carried out for the different complexes. In general, ωB97X-D functionals, with higher ratios of long-range Hartree–Fock exchange usually provide better descriptions for charge-transfer states.

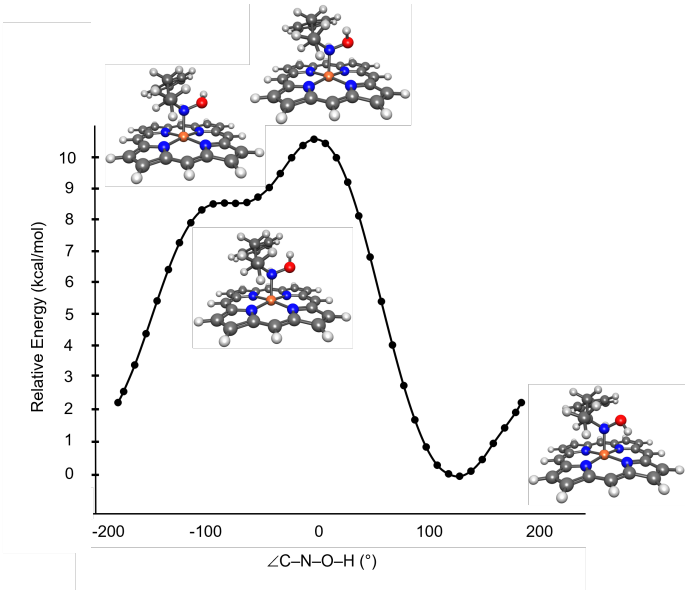

Figure S6. Potential energy surface for the 5-coordinate ferrous complex (por)Fe^{II}(AmphNHOH) using ωB97X-D/6-31+G*.

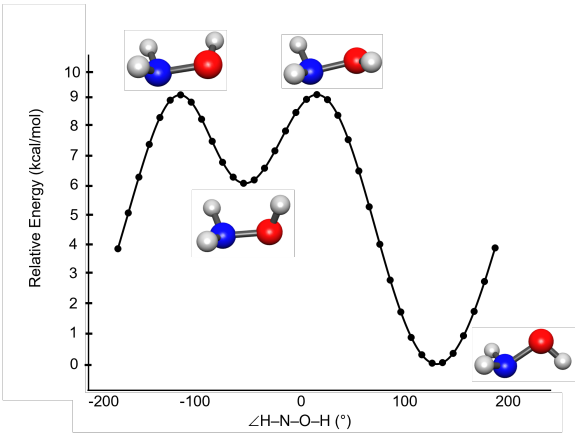

Figure S7. Potential energy surface for NH_2OH using ωB97X-D/6-31+G*.

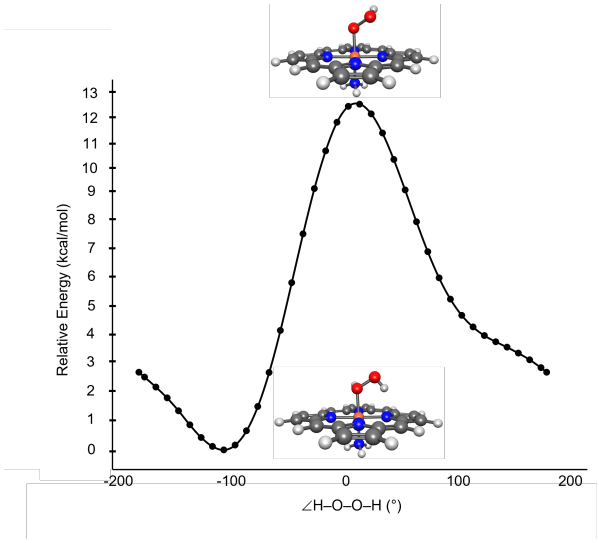

Figure S8. Potential energy surface for the ferrous complex (por)$Fe^{II}(H_2O_2)(NH_3)$ using ωB97X-D/6-31+G*.

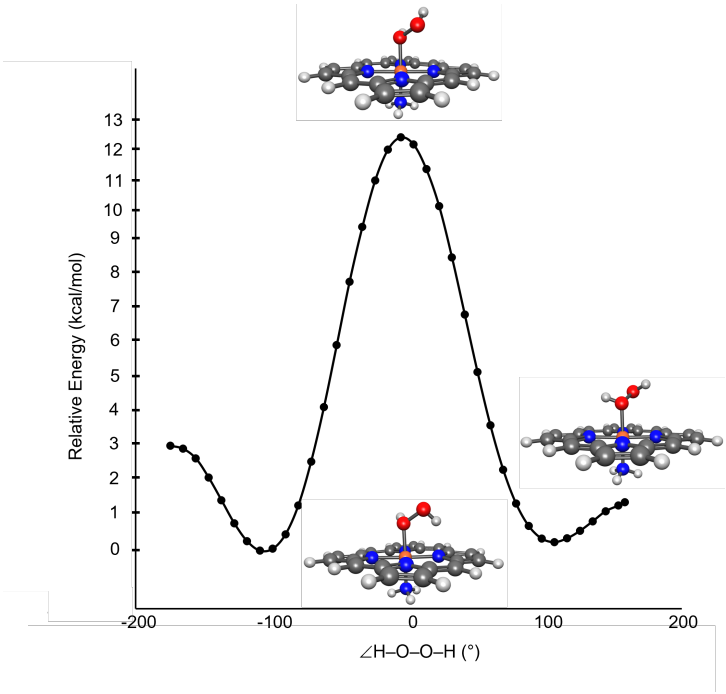

Figure S9. Potential energy surface for the ferric complex (por)$Fe^{III}(H_2O_2)(NH_3)$ using ωB97X-D/6-31+G*.

Table S2. Selected bond lengths (in Å) of -OH down-and-up conformation of (TPP)Fe^{II}(AmphNHOH)(AmphNO) using ωB97X-D/LANL2DZ-6-31+G*.[a]

Structure	Bonds	Down	Up
FREE LIGAND	O3-H4	0.96430	0.97249
	O3-N10	1.43230	1.41636
	N10-H11	1.01988	1.01972
	N10-C104	1.46546	1.46337
COMPLEX	O3-H4	0.97269	0.97127
	O3-N10	1.42340	1.41906
	N10-H11	1.02181	1.02160
	N10-C104	1.47752	1.47775
	N10-Fe1	2.15445	2.13976
	Fe1-N8	2.03565	2.01588
	N8-C33	1.37354	1.36649
	N8-H4	1.97177	3.89222

[a] "Down" and "up" refer to the position of the hydroxyl H-atom with respect to the porphyrin; "down" represents the H-bonding interaction.

Table S3. Deviations (in Å) of the metall and 4 N(por) atoms from the 24-atom mean porphyrin plane.

Complex	Number	Experimental	Theoretical (ωB97X-D/LANL2DZ-6-31+G*)
(TPP)Fe(AmphNHOH)(NOAmph)	Fe	0.043	0.009
	N1	0.059	0.016
	N2	-0.021	-0.017
	N3	-0.011	-0.036
	N4	-0.085	-0.060
(TPP)Co(AmphNHOH)	Co	0.130	0.094
	N1	-0.019	-0.035
	N2	0.019	0.003
	N3	-0.044	-0.001
	N4	0.167	0.058

Nitrogen highlighted in red is involved in H-bonding

Table S4. Selected Mayer bond orders of -OH down-and-up conformation of (TPP)Fe^{II}(AmphNHOH)(AmphNO) using ωB97X-D/LANL2DZ-6-31+G*.[a]

Structure	Bonds	Down	Up
FREE LIGAND	O3-H4	0.69121	0.67589
	O3-N10	1.09152	1.04312
	N10-H11	0.77351	0.76304
	N10-C104	1.08705	1.21658
COMPLEX	O3-H4	0.40828	0.56066
	O3-N10	1.07797	1.66644
	N10-H11	0.75052	0.72752
	N10-C104	0.31274	0.54219
	N10-Fe1	-1.12238	-0.48946
	Fe1-N8	0.21975	-0.39395
	N8-C33	1.37365	1.37610
	N8-H4	0.17339	-0.00976

[a] "Down" and "up" refer to the position of the hydroxyl H-atom with respect to the porphyrin; "down" represents the H-bonding interaction.

Table S5. Optimized energies for different spin states of ferrous (por)$Fe^{II}(NH_2OH)(NH_3)$ and ferric (por)Fe^{III}($NH_2OH)(NH_3)$ using ωB97X-D/6-31+G*.

	(por)$Fe^{II}(NH_2OH)(NH_3)$			**(por)$Fe^{III}(NH_2OH)(NH_3)$**		
	Spin	**N-bound (kcal/mol)**	**O-bound (kcal/mol)**	**Spin**	**N-bound (kcal/mol)**	**O-bound (kcal/mol)**
Low spin	Singlet	0	10.53	Doublet	0	10.15
High spin	Triplet	26.33	16.35	Quartet	38.21	9.19
	Quintet	10.99	15.82	Sextet	41.79	16.25

Table S6. Optimized energies for different spin states of ferrous (por)$Fe^{II}(H_2O_2)(NH_3)$ and ferric (por)$Fe^{III}(H_2O_2)(NH_3)$ using ωB97X-D/6-31+G*.

	Spin	**(por)$Fe^{II}(H_2O_2)(NH_3)$ (kcal/mol)**	**Spin**	**(por)$Fe^{III}(H_2O_2)(NH_3)$ (kcal/mol)**
Low spin	Singlet	0	Doublet	0
High spin	Triplet	4.37	Quartet	39.06
	Quintet	4.02	Sextet	4.72

Table S7. Natural Bond Orbital Analysis for (TPP)Fe^{II}(NH_2OH)(AmphNO) using ωB97X-D/LANL2DZ-6-31+G*.[a]

	Conformation	Donor NBO	Acceptor NBO	E (kcal/mol)
Iron	H "down"	π N8-C33	σ* O3-H4	2.32
		σ N10	*d** Fe	34.44
		σ N9	*d** Fe (trans)	52.59
	H "up"	π N8-C33	σ* O3- H4	-
		σ N10	*d** Fe	31.58
		σ N9	*d** Fe (trans)	52.84

[a] "Down" and "up" refer to the position of the hydroxyl H-atom with respect to the porphyrin; "down" represents the H-bonding interaction.
π = bonding orbital; located on a porphyrin pyrrole N=C fragment.
σ* = antibonding orbital; located on the hydroxyl OH group. Atom numbering refers to the calculated structures.

References:

[1] H. B. Hass, A. G. Susie, R. L. Heider, *J. Org. Chem.* **1950**, *15*, 8-14.
[2] R. Calheiros, N. Milhazes, F. Borges, M. P. M. Marques, *J. Mol. Struct.* **2004**, *692*, 91-106.
[3] M. S. Mourad, R. S. Varma, G. W. Kabalka, *J. Org. Chem.* **1985**, *50*, 133-135.
[4] APEX2, Bruker-AXS, Madison, WI, **2007**.
[5] SAINT, *Data Reduction: SAINT Software Reference Manual. Bruker-AXS, Madison, WI.* **2007**.
[6] G. M. Sheldrick, *Acta Cryst.* **2015**, *A71*, 3-8.
[7] G. M. Sheldrick, *Acta Cryst.* **2015**, *C71*, 3-8.
[8] L. Krause, R. Herbst-Irmer, G. M. Sheldrick, D. Stalke, *J. Appl. Cryst.* **2015**, *48*, 3-10.
[9] R. G. Parr, W. Yang, *Density-Functional Theory of Atoms and Molecules*, Oxford University Press, New York, **1989**.
[10] A. D. Becke, *J. Chem. Phys.* **2014**, *140*, 18A301.
[11] E. Epifanovsky, A. T. B. Gilbert, X. Feng, J. Lee, Y. Mao, N. Mardirossian, P. Pokhilko, A. F. White, M. P. Coons, A. L. Dempwolff, Z. Gan, D. Hait, P. R. Horn, L. D. Jacobson, I. Kaliman, J. Kussmann, A. W. Lange, K. U. Lao, D. S. Levine, J. Liu, S. C. McKenzie, A. F. Morrison, K. D. Nanda, F. Plasser, D. R. Rehn, M. L. Vidal, Z.-Q. You, Y. Zhu, B. Alam, B. J. Albrecht, A. Aldossary, E. Alguire, J. H. Andersen, V. Athavale, D. Barton, K. Begam, A. Behn, N. Bellonzi, Y. A. Bernard, E. J. Berquist, H. G. A. Burton, A. Carreras, K. Carter-Fenk, R. Chakraborty, A. D. Chien, K. D. Closser, V. Cofer-Shabica, S. Dasgupta, M. de Wergifosse, J. Deng, M. Diedenhofen, H. Do, S. Ehlert, P.-T. Fang, S. Fatehi, Q. Feng, T. Friedhoff, J. Gayvert, Q. Ge, G. Gidofalvi, M. Goldey, J. Gomes, C. E. González-Espinoza, S. Gulania, A. O. Gunina, M. W. D. Hanson-Heine, P. H. P. Harbach, A. Hauser, M. F. Herbst, M. Hernández Vera, M. Hodecker, Z. C. Holden, S. Houck, X. Huang, K. Hui, B. C. Huynh, M. Ivanov, Á. Jász, H. Ji, H. Jiang, B. Kaduk, S. Kähler, K. Khistyaev, J. Kim, G. Kis, P. Klunzinger, Z. Koczor-Benda, J. H. Koh, D. Kosenkov, L. Koulias, T. Kowalczyk, C. M. Krauter, K. Kue, A. Kunitsa, T. Ku´s, I. Ladjánszki, A. Landau, K. V. Lawler, D. Lefrancois, S. Lehtola, R. R. Li, Y.-P. Li, J. Liang, M. Liebenthal, H.-H. Lin, Y.-S. Lin, F. Liu, K.-Y. Liu, M. Loipersberger, A. Luenser, A. Manjanath, P. Manohar, E. Mansoor, S. F. Manzer, S.-P. Mao, A. V. Marenich, T. Markovich, S. Mason, S. A. Maurer, P. F. McLaughlin, M. F. S. J. Menger, J.-M. Mewes, S. Mewes, P. Morgante, J. W. Mullinax, K. J. Oosterbaan, G. Paran, A. C. Paul, S. K. Paul, F. Pavo˘sevic, Z. Pei, S. Prager, E. I. Proynov, Á. Rák, E. Ramos- ´ Cordoba, B. Rana, A. E. Rask, A. Rettig, R. M. Richards, F. Rob, E. Rossomme, T. Scheele, M. Scheurer, M. Schneider, N. Sergueev, S. M. Sharada, W. Skomorowski, D. W. Small, C. J. Stein, Y.-C. Su, E. J. Sundstrom, Z. Tao, J. Thirman, G. J. Tornai, T. Tsuchimochi, N. M. Tubman, S. P. Veccham, O. Vydrov, J. Wenzel, J. Witte, A. Yamada, K. Yao, S. Yeganeh, S. R. Yost, A. Zech, I. Y. Zhang, X. Zhang, Y. Zhang, D. Zuev, A. Aspuru-Guzik, A. T. Bell, N. A. Besley, K. B. Bravaya, B. R. Brooks, D. Casanova, J.-D. Chai, S. Coriani, C. Cramer, G. Cserey, A. E. DePrince III, R. A. DiStasio, Jr., A. Dreuw, B. D. Dunietz, T. R. Furlani, W. A. Goddard III, S. Hammes-Schiffer, T. Head-Gordon, W. J. Hehre, C.-P. Hsu, T.-C. Jagau, Y. Jung, A. Klamt, J. Kong, D. S. Lambrecht, W. Liang, N. J. Mayhall, C. W. McCurdy, J. B. Neaton, C. Ochsenfeld, J. A. Parkhill, R. Peverati, V. A. Rassolov, Y. Shao, L. V. Slipchenko, T. Stauch, R. P. Steele, J. E. Subotnik, A. J. W. Thom, A. Tkatchenko, D. G. Truhlar, T. Van Voorhis, T. A. Wesolowski, K. B. Whaley, H. L. Woodcock III, P. M. Zimmerman, S. Faraji, P. M. W. Gill, M. Head-Gordon, J. M. Herbert, and A. I. Krylov,, *J. Chem. Phys.* **2021**, *155*, 084801-084859.
[12] J.-D. Chai, M. Head-Gordon, *Phys. Chem. Chem. Phys.* **2008**, *10*, 6615-6620.
[13] P. J. Hay, W. R. Wadt, *J. Chem. Phys.* **1985**, *82*, 299-310.
[14] W. J. Hehre, R. Ditchfield, J. A. Pople, *J. Chem. Phys.* **1972**, *56*, 2257-2261.
[15] P. C. Hariharan, J. A. Pople, *Theor. Chim. Acta* **1973**, *28*, 213-222.

CARTESIAN COORDINATES FOR THE COMPUTED STRUCTURES

Table S8: *OH-down*-(TPP)Fe^{II}(AmphNHOH)(AmphNO)

ATOM		X	Y	Z
1	Fe	-0.123184	-0.116955	0.006786
2	O	-0.166805	0.154999	-2.712110
3	O	-0.421253	0.791608	2.884619
4	H	0.401890	1.021458	2.420155
5	N	-1.216519	1.537253	-0.364756
6	N	-1.644532	-1.267512	-0.600579
7	N	0.978264	-1.753768	0.422886
8	N	1.388509	1.049066	0.713204
9	N	0.533202	-0.057760	-1.747138
10	N	-1.068561	-0.055804	1.941772
11	H	-1.866710	0.499686	1.627936
12	C	-0.804500	2.834803	-0.252975
13	C	-1.850202	3.730906	-0.694375
14	H	-1.783773	4.810249	-0.699320
15	C	-2.887040	2.954786	-1.089735
16	H	-3.841674	3.270085	-1.487368
17	C	-2.479629	1.583137	-0.886145
18	C	-3.265484	0.478283	-1.215991
19	C	-2.860329	-0.849248	-1.058744
20	C	-3.688526	-1.987471	-1.387602
21	H	-4.705037	-1.933058	-1.751876
22	C	-2.944886	-3.093150	-1.144324
23	H	-3.226033	-4.129443	-1.271894
24	C	-1.661426	-2.631680	-0.665905
25	C	-0.608286	-3.480904	-0.320732
26	C	0.619240	-3.051480	0.185952
27	C	1.677722	-3.945606	0.594733
28	H	1.651707	-5.023145	0.509495
29	C	2.668124	-3.170906	1.100498
30	H	3.614712	-3.488370	1.515420
31	C	2.224227	-1.801226	0.984216
32	C	2.987979	-0.700258	1.382618
33	C	2.588897	0.629026	1.232096
34	C	3.421817	1.766719	1.532566
35	H	4.417690	1.716022	1.951515
36	C	2.726838	2.873314	1.164303
37	H	3.040078	3.906392	1.226546
38	C	1.456113	2.420358	0.657920
39	C	0.442815	3.266661	0.204891
40	C	-4.601720	0.724190	-1.838168
41	C	-4.777553	0.546876	-3.213886
42	H	-3.931109	0.235384	-3.820456
43	C	-6.021763	0.767769	-3.800940
44	H	-6.146242	0.626344	-4.871113
45	C	-7.104077	1.169015	-3.018190
46	H	-8.075142	1.337250	-3.475624
47	C	-6.933391	1.350716	-1.646716
48	H	-7.771265	1.661114	-1.027855
49	C	-5.688156	1.130161	-1.061479
50	H	-5.549764	1.266829	0.006052
51	C	-0.818062	-4.952035	-0.484160
52	C	-0.724244	-5.548175	-1.744592
53	H	-0.495281	-4.927932	-2.607495
54	C	-0.922381	-6.919155	-1.895763
55	H	-0.846267	-7.370935	-2.880937
56	C	-1.218353	-7.709130	-0.785926
57	H	-1.374116	-8.777832	-0.903846
58	C	-1.314382	-7.122021	0.475035
59	H	-1.546479	-7.732063	1.343648
60	C	-1.114853	-5.751260	0.623618
61	H	-1.186095	-5.288306	1.604778
62	C	4.354659	-0.948695	1.933271
63	C	5.405269	-1.287499	1.074642
64	H	5.211760	-1.382398	0.009114
65	C	6.689411	-1.493450	1.573625
66	H	7.495395	-1.752772	0.892612
67	C	6.937695	-1.363162	2.939510
68	H	7.939140	-1.521051	3.329931
69	C	5.894825	-1.029575	3.802476
70	H	6.080368	-0.927979	4.868211
71	C	4.610678	-0.823493	3.301185
72	H	3.796353	-0.561547	3.971865
73	C	0.718007	4.736068	0.202157
74	C	1.072033	5.381822	-0.985891
75	H	1.135099	4.803843	-1.904414
76	C	1.337004	6.749532	-0.997405
77	H	1.614678	7.237404	-1.927534
78	C	1.250833	7.487622	0.182121
79	H	1.458323	8.553982	0.174698
80	C	0.896385	6.851613	1.371017

81	H	0.827602	7.420400	2.294143
82	C	0.631465	5.483423	1.380056
83	H	0.352738	4.984705	2.304933
84	C	1.973078	-0.275226	-2.080035
85	H	2.473408	-0.445068	-1.130594
86	C	2.097924	-1.518113	-2.953632
87	H	1.594008	-1.373585	-3.914609
88	H	1.657888	-2.383424	-2.446838
89	H	3.156071	-1.726351	-3.136972
90	C	2.529509	1.012989	-2.711342
91	H	2.031830	1.187077	-3.671416
92	H	2.284037	1.853528	-2.049851
93	C	4.025162	0.915355	-2.888004
94	C	4.866968	0.990126	-1.773441
95	H	4.436130	1.164213	-0.790458
96	C	6.244486	0.842667	-1.907620
97	H	6.877423	0.897798	-1.025696
98	C	6.805081	0.624514	-3.165957
99	H	7.880194	0.511035	-3.274613
100	C	5.977110	0.557507	-4.284824
101	H	6.404939	0.393934	-5.270222
102	C	4.596815	0.699308	-4.144042
103	H	3.956301	0.640503	-5.021380
104	C	-1.627322	-1.207300	2.679947
105	H	-2.154213	-1.783443	1.910356
106	C	-0.538808	-2.056804	3.323339
107	H	0.173945	-2.426363	2.587986
108	H	-0.995917	-2.917634	3.823541
109	H	0.006442	-1.474501	4.072451
110	C	-2.636710	-0.753560	3.758903
111	H	-3.049715	-1.659318	4.217966
112	H	-2.080198	-0.224440	4.540587
113	C	-3.768274	0.118321	3.269235
114	C	-5.022913	-0.428498	2.980570
115	H	-5.176267	-1.500066	3.090501
116	C	-6.082981	0.382193	2.581479
117	H	-7.053931	-0.060229	2.375495
118	C	-5.897605	1.757145	2.444629
119	H	-6.723350	2.392617	2.135614
120	C	-4.643530	2.311054	2.693805
121	H	-4.483699	3.378666	2.571261
122	C	-3.590943	1.498964	3.111654
123	H	-2.620563	1.938936	3.332407

Table S9: *OH-up*-(TPP)Fe^{II}(AmphNHOH)(AmphNO)

ATOM		X	Y	Z
1	Fe	-0.126587	-0.085233	-0.036182
2	O	-0.284014	0.275873	-2.745045
3	O	-0.419866	1.000728	2.756407
4	H	-1.150985	1.383524	3.268566
5	N	-0.725065	1.827559	-0.200020
6	N	-1.948597	-0.710049	-0.632473
7	N	0.480510	-2.006396	0.128640
8	N	1.647536	0.520874	0.704691
9	N	0.435225	-0.039793	-1.823134
10	N	-0.993445	0.010036	1.917796
11	H	-1.864393	0.411622	1.565885
12	C	0.044252	2.936689	0.015222
13	C	-0.655266	4.119453	-0.435425
14	H	-0.261565	5.125930	-0.409173
15	C	-1.858019	3.707697	-0.902225
16	H	-2.645163	4.310378	-1.333107
17	C	-1.896962	2.270885	-0.742409
18	C	-2.988040	1.471589	-1.098799
19	C	-2.998794	0.076358	-1.015565
20	C	-4.137071	-0.747401	-1.352390
21	H	-5.103451	-0.379117	-1.667660
22	C	-3.750252	-2.036212	-1.192366
23	H	-4.334959	-2.931872	-1.350988
24	C	-2.368772	-2.004175	-0.768471
25	C	-1.580490	-3.143293	-0.589281
26	C	-0.235680	-3.120232	-0.207347
27	C	0.591729	-4.299294	-0.092609
28	H	0.276417	-5.308613	-0.318620
29	C	1.809294	-3.881429	0.333307
30	H	2.687051	-4.480978	0.531742
31	C	1.724258	-2.449042	0.490572
32	C	2.741222	-1.656589	1.026860
33	C	2.650387	-0.271824	1.187615
34	C	3.656841	0.534210	1.837994
35	H	4.543012	0.150688	2.325023
36	C	3.262388	1.824721	1.708494
37	H	3.755454	2.713624	2.076834

38	C	2.013874	1.804996	0.981202
39	C	1.313129	2.951893	0.597209
40	C	-4.206594	2.145561	-1.635456
41	C	-4.584083	1.963728	-2.970420
42	H	-3.970657	1.335088	-3.610466
43	C	-5.726236	2.579736	-3.476564
44	H	-6.003463	2.427865	-4.516122
45	C	-6.506823	3.391015	-2.654139
46	H	-7.399409	3.868881	-3.047870
47	C	-6.132879	3.587233	-1.325428
48	H	-6.733659	4.221613	-0.678987
49	C	-4.989565	2.970657	-0.821753
50	H	-4.697697	3.120945	0.213731
51	C	-2.210286	-4.476627	-0.833836
52	C	-2.465991	-4.917131	-2.135995
53	H	-2.202814	-4.274565	-2.972266
54	C	-3.050044	-6.161865	-2.362188
55	H	-3.241292	-6.490278	-3.380087
56	C	-3.386741	-6.982387	-1.286549
57	H	-3.842264	-7.953147	-1.460902
58	C	-3.135346	-6.551954	0.015387
59	H	-3.394657	-7.186376	0.858473
60	C	-2.549906	-5.307333	0.238273
61	H	-2.348034	-4.972522	1.252885
62	C	4.001173	-2.327519	1.464527
63	C	5.167183	-2.204216	0.702436
64	H	5.144712	-1.619298	-0.213873
65	C	6.346085	-2.826198	1.108100
66	H	7.243571	-2.727175	0.503637
67	C	6.373318	-3.575787	2.283571
68	H	7.293049	-4.057593	2.603290
69	C	5.215173	-3.702647	3.049365
70	H	5.229557	-4.281815	3.968520
71	C	4.035955	-3.083725	2.639808
72	H	3.131093	-3.178496	3.234842
73	C	1.976230	4.271820	0.811079
74	C	3.113359	4.615667	0.071386
75	H	3.506023	3.910445	-0.657405
76	C	3.735866	5.847608	0.258321
77	H	4.613408	6.102391	-0.329462
78	C	3.231291	6.751359	1.192373
79	H	3.715626	7.713078	1.336756
80	C	2.101773	6.415913	1.937730
81	H	1.706264	7.114100	2.670395
82	C	1.479022	5.184234	1.747074
83	H	0.599806	4.918527	2.328225
84	C	1.838553	-0.344983	-2.228994
85	H	2.341494	-0.684897	-1.327568
86	C	1.857015	-1.447977	-3.277892
87	H	1.331991	-1.137260	-4.186320
88	H	1.385317	-2.353962	-2.882112
89	H	2.894778	-1.685783	-3.530811
90	C	2.467050	0.989186	-2.676739
91	H	2.015218	1.295701	-3.626566
92	H	2.213675	1.750967	-1.929289
93	C	3.964828	0.871370	-2.797503
94	C	4.762067	0.927372	-1.649674
95	H	4.295057	1.091064	-0.681532
96	C	6.143071	0.770459	-1.732403
97	H	6.742720	0.814326	-0.826799
98	C	6.750175	0.557761	-2.969965
99	H	7.827819	0.436665	-3.038146
100	C	5.965851	0.508124	-4.121036
101	H	6.430534	0.350726	-5.090621
102	C	4.582932	0.663236	-4.032921
103	H	3.976293	0.623596	-4.935107
104	C	-1.340857	-1.196943	2.696414
105	H	-1.729623	-1.885143	1.938022
106	C	-0.115710	-1.808082	3.359746
107	H	0.631952	-2.089485	2.620519
108	H	-0.410511	-2.703379	3.918460
109	H	0.337216	-1.096594	4.057078
110	C	-2.437087	-0.931526	3.752747
111	H	-2.829298	-1.906535	4.068132
112	H	-1.977713	-0.488501	4.645812
113	C	-3.567583	-0.047548	3.280755
114	C	-4.327957	-0.385747	2.154147
115	H	-4.107132	-1.296160	1.600133
116	C	-5.355872	0.443438	1.716730
117	H	-5.923251	0.172190	0.831371
118	C	-5.645889	1.624702	2.398604
119	H	-6.450858	2.267981	2.054580
120	C	-4.891038	1.979272	3.512893
121	H	-5.103700	2.900369	4.048439
122	C	-3.857116	1.148146	3.945283
123	H	-3.280213	1.424058	4.826899

Table S10: *OH-down*-(TPP)$Fe^{II}(NH_2OH)$(AmphNO)

ATOM		X	Y	Z
1	Fe	0.569019	-0.033767	0.533356
2	O	1.027996	-0.458104	-2.136260
3	O	0.168932	-0.538455	3.471926
4	H	-0.568197	-0.827540	2.905837
5	N	1.377820	-1.869408	0.412359
6	N	2.368774	0.794813	0.216841
7	N	-0.249354	1.802867	0.758539
8	N	-1.236328	-0.866364	0.962924
9	N	0.233742	-0.053700	-1.316269
10	N	1.071460	0.001142	2.526567
11	H	1.941912	-0.514005	2.651498
12	H	1.235356	0.963556	2.819443
13	C	0.714720	-3.062584	0.437330
14	C	1.645524	-4.155760	0.262876
15	H	1.381070	-5.204174	0.252144
16	C	2.873999	-3.602670	0.129525
17	H	3.818539	-4.106477	-0.021954
18	C	2.695095	-2.169939	0.214799
19	C	3.731853	-1.246044	0.059683
20	C	3.555179	0.139297	0.043824
21	C	4.621464	1.091142	-0.173309
22	H	5.662825	0.839818	-0.319696
23	C	4.055675	2.322013	-0.154384
24	H	4.540081	3.281011	-0.277476
25	C	2.645224	2.126643	0.094200
26	C	1.726218	3.171000	0.229174
27	C	0.381820	3.001163	0.566906
28	C	-0.541467	4.091979	0.782402
29	H	-0.300882	5.141994	0.687977
30	C	-1.728192	3.535864	1.125848
31	H	-2.651558	4.039622	1.375904
32	C	-1.540727	2.102695	1.097483
33	C	-2.562989	1.178970	1.331314
34	C	-2.408617	-0.207286	1.239750
35	C	-3.492169	-1.152110	1.346081
36	H	-4.522838	-0.898130	1.553586
37	C	-2.968927	-2.382075	1.107792
38	H	-3.487127	-3.330666	1.086779
39	C	-1.558204	-2.198934	0.877452
40	C	-0.659556	-3.236699	0.621644
41	C	5.112991	-1.779690	-0.145489
42	C	5.697149	-1.769063	-1.415628
43	H	5.135193	-1.365502	-2.253767
44	C	6.982130	-2.272669	-1.607243
45	H	7.424648	-2.260280	-2.599445
46	C	7.698169	-2.793128	-0.530073
47	H	8.699908	-3.186235	-0.679280
48	C	7.122730	-2.808254	0.739299
49	H	7.672912	-3.212872	1.584212
50	C	5.837532	-2.304182	0.928693
51	H	5.384663	-2.316951	1.916798
52	C	2.224001	4.564493	0.012757
53	C	2.381875	5.058809	-1.285314
54	H	2.139607	4.417082	-2.128632
55	C	2.845903	6.355171	-1.498698
56	H	2.961702	6.727195	-2.512939
57	C	3.159243	7.172444	-0.413700
58	H	3.521127	8.183354	-0.578769
59	C	3.006187	6.686937	0.884201
60	H	3.250329	7.318357	1.733972
61	C	2.540350	5.390591	1.094864
62	H	2.421017	5.009388	2.105894
63	C	-3.935294	1.701754	1.609076
64	C	-4.699974	2.245659	0.571898
65	H	-4.279322	2.292125	-0.429355
66	C	-5.988414	2.716720	0.812848
67	H	-6.569849	3.135243	-0.004124
68	C	-6.527697	2.649033	2.096896
69	H	-7.533052	3.014347	2.286754
70	C	-5.771498	2.110253	3.136806
71	H	-6.185926	2.057173	4.139731
72	C	-4.482499	1.638831	2.893523
73	H	-3.891512	1.217126	3.702443
74	C	-1.203506	-4.626318	0.540061
75	C	-1.340729	-5.251538	-0.702971
76	H	-1.044750	-4.714655	-1.600676
77	C	-1.848220	-6.545714	-0.793823
78	H	-1.948625	-7.018816	-1.766696
79	C	-2.224962	-7.230935	0.360289
80	H	-2.622670	-8.239520	0.291326
81	C	-2.090127	-6.615629	1.603964
82	H	-2.379983	-7.144349	2.507794
83	C	-1.582284	-5.320914	1.692521

84	H	-1.475927	-4.839456	2.661353
85	C	-1.042497	0.451109	-1.907705
86	H	-1.656657	0.762600	-1.066536
87	C	-0.734407	1.656776	-2.788685
88	H	-0.099551	1.369963	-3.633074
89	H	-0.225328	2.431867	-2.206179
90	H	-1.669989	2.072212	-3.174128
91	C	-1.744411	-0.710217	-2.632779
92	H	-1.131370	-1.026122	-3.483680
93	H	-1.814609	-1.557875	-1.939254
94	C	-3.124724	-0.300596	-3.085551
95	C	-4.152898	-0.148200	-2.149629
96	H	-3.958549	-0.369919	-1.103021
97	C	-5.416941	0.283252	-2.541797
98	H	-6.198441	0.402854	-1.795878
99	C	-5.675454	0.563130	-3.883457
100	H	-6.661767	0.897261	-4.193087
101	C	-4.661212	0.406442	-4.826113
102	H	-4.854312	0.617156	-5.874449
103	C	-3.394689	-0.019460	-4.426894
104	H	-2.606033	-0.137001	-5.166898

Table S11: *OH-up*-(TPP)Fe^{II}(NH_2OH)(AmphNO)

ATOM	X	Y	Z
1 Fe	-0.546959	0.023486	0.488499
2 O	-1.132381	0.319558	-2.168652
3 O	-0.034665	0.556826	3.403158
4 H	-0.425235	0.523788	4.289880
5 N	-1.137638	1.940729	0.358564
6 N	-2.451615	-0.591556	0.266617
7 N	0.040416	-1.903528	0.697301
8 N	1.343258	0.627869	0.856271
9 N	-0.303535	-0.043581	-1.362808
10 N	-1.001917	0.061754	2.500589
11 H	-1.840942	0.637507	2.573335
12 H	-1.227867	-0.899081	2.759372
13 C	-0.328033	3.041641	0.317938
14 C	-1.109809	4.220970	0.017897
15 H	-0.712839	5.219704	-0.099848
16 C	-2.399506	3.818681	-0.084116
17 H	-3.270361	4.421250	-0.302858
18 C	-2.406069	2.388569	0.127194
19 C	-3.557469	1.597206	0.072584
20 C	-3.557748	0.202001	0.139607
21 C	-4.743396	-0.615554	0.014321
22 H	-5.753543	-0.239889	-0.073356
23 C	-4.329926	-1.906107	0.020001
24 H	-4.932735	-2.800478	-0.058279
25 C	-2.892619	-1.882309	0.170102
26 C	-2.092442	-3.027503	0.207804
27 C	-0.716829	-3.017433	0.458969
28 C	0.104382	-4.203314	0.536253
29 H	-0.239501	-5.214299	0.366646
30 C	1.356428	-3.790641	0.855782
31 H	2.241224	-4.395512	1.000140
32 C	1.306397	-2.351811	0.959598
33 C	2.408627	-1.549988	1.263952
34 C	2.392637	-0.153822	1.249610
35 C	3.529561	0.668861	1.589141
36 H	4.479508	0.299394	1.950741
37 C	3.159158	1.953476	1.365715
38 H	3.743093	2.851472	1.512284
39 C	1.789824	1.915158	0.903257
40 C	1.044486	3.052797	0.575553
41 C	-4.869142	2.285731	-0.129131
42 C	-5.493373	2.268975	-1.380126
43 H	-5.007996	1.754821	-2.205471
44 C	-6.719147	2.903809	-1.569113
45 H	-7.192767	2.883608	-2.546707
46 C	-7.336884	3.563617	-0.507321
47 H	-8.294335	4.056232	-0.651941
48 C	-6.719964	3.588975	0.742230
49 H	-7.194628	4.100380	1.575148
50 C	-5.492794	2.955100	0.927872
51 H	-5.009202	2.974404	1.901318
52 C	-2.750544	-4.346359	-0.040426
53 C	-3.146235	-4.695332	-1.335799
54 H	-2.969945	-3.994248	-2.147533
55 C	-3.755836	-5.922661	-1.586169
56 H	-4.053106	-6.180587	-2.598891
57 C	-3.980028	-6.817665	-0.541082

58	H	-4.455317	-7.775359	-0.733876
59	C	-3.592137	-6.477753	0.754088
60	H	-3.767368	-7.169596	1.573281
61	C	-2.981013	-5.249939	1.001370
62	H	-2.679300	-4.983816	2.011290
63	C	3.703663	-2.231873	1.566186
64	C	4.694188	-2.324363	0.583377
65	H	4.513927	-1.888208	-0.396300
66	C	5.899568	-2.968729	0.853224
67	H	6.657722	-3.040597	0.078095
68	C	6.128646	-3.526086	2.110914
69	H	7.068237	-4.029333	2.321327
70	C	5.147089	-3.434872	3.096595
71	H	5.319130	-3.865273	4.079422
72	C	3.940249	-2.793188	2.823566
73	H	3.172023	-2.717796	3.588843
74	C	1.768279	4.357831	0.532962
75	C	2.710758	4.605575	-0.470858
76	H	2.900988	3.842605	-1.221808
77	C	3.403094	5.813520	-0.512746
78	H	4.131000	5.991467	-1.299405
79	C	3.163407	6.790568	0.452280
80	H	3.704154	7.732260	0.422539
81	C	2.227153	6.552719	1.457545
82	H	2.037450	7.307419	2.215832
83	C	1.534924	5.344348	1.496360
84	H	0.808178	5.153509	2.281594
85	C	0.958123	-0.552280	-1.977620
86	H	1.595910	-0.843910	-1.146792
87	C	0.655071	-1.768163	-2.843718
88	H	-0.015099	-1.504249	-3.667933
89	H	0.189933	-2.557411	-2.243691
90	H	1.590405	-2.159092	-3.255723
91	C	1.615908	0.623024	-2.724859
92	H	1.048348	0.830500	-3.638559
93	H	1.549308	1.513566	-2.087885
94	C	3.062684	0.329979	-3.031152
95	C	4.032301	0.525121	-2.042425
96	H	3.733548	0.914336	-1.072076
97	C	5.369623	0.223614	-2.285236
98	H	6.107196	0.385973	-1.503508
99	C	5.758429	-0.280915	-3.526010
100	H	6.801855	-0.513514	-3.720174
101	C	4.800653	-0.477166	-4.519506
102	H	5.096347	-0.865002	-5.490493
103	C	3.462563	-0.173122	-4.271737
104	H	2.719300	-0.328429	-5.050819

Table S12: *OH-down-(*por)Fe^{II}(AmphNHOH)(NH_3)

ATOM		X	Y	Z
1	Fe	-0.843402	0.053059	0.567548
2	O	-0.470152	0.671580	-2.321129
3	H	-1.368177	0.845597	-1.994291
4	N	-0.041066	1.896394	0.675122
5	N	0.812774	-0.716306	1.401810
6	N	-1.668091	-1.773173	0.513736
7	N	-2.513948	0.837344	-0.243345
8	N	-1.663342	0.308067	2.416194
9	N	0.110621	-0.071735	-1.252726
10	H	0.936239	0.484068	-1.023609
11	C	-0.615414	3.072687	0.279239
12	C	0.296900	4.175049	0.480912
13	H	0.079516	5.209454	0.244770
14	C	1.432400	3.647742	1.002266
15	H	2.345515	4.155539	1.287045
16	C	1.207210	2.226367	1.125118
17	C	2.131482	1.329594	1.642394
18	C	1.935688	-0.036188	1.785265
19	C	2.902559	-0.939221	2.363131
20	H	3.874796	-0.642470	2.736024
21	C	2.348807	-2.176330	2.326799
22	H	2.766037	-3.113706	2.673739
23	C	1.044381	-2.025584	1.723899
24	C	0.157579	-3.069524	1.498786
25	C	-1.104646	-2.945401	0.932402
26	C	-2.012541	-4.049665	0.722677
27	H	-1.798068	-5.082786	0.967088
28	C	-3.140453	-3.525436	0.182123
29	H	-4.047593	-4.036268	-0.116031
30	C	-2.914786	-2.103449	0.059263
31	C	-3.839289	-1.209056	-0.463009
32	C	-3.654489	0.160700	-0.590961

33	C	-4.654200	1.077020	-1.081855
34	H	-5.639202	0.789457	-1.428027
35	C	-4.113903	2.320859	-1.008047
36	H	-4.561130	3.267010	-1.286240
37	C	-2.783519	2.163161	-0.474113
38	C	-1.894340	3.204967	-0.244121
39	C	0.611091	-1.350580	-1.808318
40	H	0.945610	-1.914768	-0.932001
41	C	-0.489089	-2.118790	-2.523501
42	H	-1.391142	-2.169740	-1.912510
43	H	-0.151770	-3.141074	-2.723948
44	H	-0.741984	-1.643804	-3.475646
45	C	1.823876	-1.112304	-2.729761
46	H	2.177628	-2.089488	-3.079863
47	H	1.491489	-0.553358	-3.611748
48	C	2.942717	-0.375674	-2.033775
49	C	3.811909	-1.051945	-1.172588
50	H	3.696645	-2.124597	-1.030677
51	C	4.813367	-0.370282	-0.488543
52	H	5.478413	-0.917623	0.173668
53	C	4.954479	1.007489	-0.644597
54	H	5.736306	1.540895	-0.110600
55	C	4.084082	1.696501	-1.485036
56	H	4.176872	2.772438	-1.605296
57	C	3.087636	1.008300	-2.175516
58	H	2.406478	1.552548	-2.826335
59	H	-2.550807	-0.182206	2.512299
60	H	-1.829226	1.292312	2.618866
61	H	3.088690	1.729683	1.963216
62	H	0.474740	-4.065721	1.795287
63	H	-4.793703	-1.613655	-0.788863
64	H	-2.225516	4.207502	-0.500556
65	H	-1.036744	-0.049157	3.135226

Table S13: *OH-down*-(por)Fe^{II}(AmphNHOH)

ATOM		X	Y	Z
1	Fe	-0.827256	0.094564	0.611310
2	O	-0.427321	0.999470	-2.120779
3	H	-1.278734	1.279479	-1.746830
4	N	0.183991	1.782499	0.992659
5	N	0.674759	-0.972963	1.386543
6	N	-1.935431	-1.561507	0.488781
7	N	-2.417535	1.191066	0.058104
8	N	0.061624	0.072590	-1.154320
9	H	0.967817	0.475508	-0.905804
10	C	-0.225208	3.069331	0.760057
11	C	0.831156	4.003713	1.062917
12	H	0.750454	5.079220	0.965624
13	C	1.891709	3.268043	1.478045
14	H	2.868609	3.608775	1.797322
15	C	1.476717	1.887790	1.434077
16	C	2.280858	0.821997	1.805827
17	C	1.893319	-0.506779	1.806934
18	C	2.729347	-1.593464	2.252151
19	H	3.735770	-1.479980	2.634808
20	C	2.005527	-2.728756	2.096122
21	H	2.286844	-3.748599	2.327839
22	C	0.728407	-2.331140	1.555158
23	C	-0.295448	-3.211875	1.245360
24	C	-1.539968	-2.845126	0.758506
25	C	-2.605578	-3.777401	0.483966
26	H	-2.539049	-4.849397	0.622160
27	C	-3.660237	-3.043230	0.051676
28	H	-4.644153	-3.383201	-0.246194
29	C	-3.233596	-1.665395	0.059450
30	C	-4.033636	-0.604472	-0.330488
31	C	-3.656958	0.729017	-0.309629
32	C	-4.531708	1.825341	-0.636124
33	H	-5.561295	1.719995	-0.954319
34	C	-3.817368	2.964350	-0.447323
35	H	-4.135639	3.990677	-0.580354
36	C	-2.506773	2.562146	-0.007050
37	C	-1.477934	3.438895	0.298177
38	C	0.352420	-1.203484	-1.854886
39	H	0.614429	-1.899718	-1.052584
40	C	-0.864723	-1.720930	-2.604076
41	H	-1.750342	-1.712512	-1.967203
42	H	-0.681756	-2.751864	-2.923709
43	H	-1.067541	-1.112482	-3.489784
44	C	1.571234	-1.047476	-2.784769
45	H	1.793962	-2.034363	-3.207145
46	H	1.299114	-0.391166	-3.618820

47	C	2.782173	-0.499386	-2.067981
48	C	3.579895	-1.326647	-1.272169
49	H	3.343888	-2.385886	-1.193655
50	C	4.666507	-0.810026	-0.573204
51	H	5.277046	-1.469836	0.036957
52	C	4.963454	0.549986	-0.644545
53	H	5.812040	0.953804	-0.099164
54	C	4.164114	1.388847	-1.416706
55	H	4.377318	2.452803	-1.469503
56	C	3.083740	0.865672	-2.124599
57	H	2.458316	1.523553	-2.724364
58	H	3.291545	1.048375	2.131409
59	H	-0.116191	-4.269411	1.418045
60	H	-5.046999	-0.832979	-0.648322
61	H	-1.672796	4.500296	0.173783

Table S14: OH-down-(por)$Fe^{II}(NH_2OH)(NH_3)$

ATOM	X	Y	Z
1 Fe	-0.759197	-0.106642	0.509198
2 O	-0.591333	-0.048179	-2.469485
3 H	-1.422933	0.318546	-2.123614
4 N	0.044467	1.727703	0.611436
5 N	0.901925	-0.883789	1.320213
6 N	-1.569423	-1.937412	0.402334
7 N	-2.428879	0.674750	-0.307132
8 N	-1.570218	0.159108	2.358466
9 N	0.107976	-0.397764	-1.283841
10 H	0.984707	0.120478	-1.342072
11 C	-0.528260	2.905802	0.217350
12 C	0.373586	4.011571	0.444639
13 H	0.153656	5.046922	0.215293
14 C	1.502691	3.486116	0.980710
15 H	2.406244	3.997561	1.288485
16 C	1.284630	2.061397	1.082765
17 C	2.208967	1.164875	1.601070
18 C	2.022804	-0.206009	1.717084
19 C	2.994245	-1.115878	2.276583
20 H	3.963800	-0.824420	2.661029
21 C	2.445745	-2.355395	2.213630
22 H	2.868357	-3.297428	2.540350
23 C	1.141339	-2.198719	1.615068
24 C	0.259795	-3.242884	1.369244
25 C	-1.000136	-3.115917	0.800358
26 C	-1.896908	-4.222695	0.558404
27 H	-1.677353	-5.258764	0.784949
28 C	-3.020696	-3.696618	0.011997
29 H	-3.919715	-4.207988	-0.308805
30 C	-2.805218	-2.270698	-0.080087
31 C	-3.741114	-1.373086	-0.574967
32 C	-3.568426	0.000711	-0.666801
33 C	-4.562834	0.918973	-1.163873
34 H	-5.545284	0.633064	-1.518369
35 C	-4.018261	2.160873	-1.090507
36 H	-4.459080	3.107676	-1.376522
37 C	-2.691496	1.999359	-0.549574
38 C	-1.802117	3.039254	-0.317959
39 H	0.333837	-1.385249	-1.404011
40 H	-2.433655	-0.367246	2.479619
41 H	-1.778567	1.139965	2.538006
42 H	3.154692	1.570008	1.950692
43 H	0.581917	-4.242787	1.647005
44 H	-4.689157	-1.779124	-0.916847
45 H	-2.130321	4.042286	-0.576275
46 H	-0.923588	-0.148818	3.082918

Table S15: *OH-down*-(por)$Fe^{III}(NH_2OH)(NH_3)$

ATOM	X	Y	Z
1 Fe	-0.760519	-0.099793	0.519939
2 O	-0.682114	-0.328016	-2.427254
3 H	-1.525849	0.055040	-2.130413
4 N	0.052475	1.713452	0.632322
5 N	0.898699	-0.866233	1.317656
6 N	-1.576211	-1.908906	0.398215
7 N	-2.414963	0.666526	-0.311272
8 N	-1.570107	0.162668	2.329388
9 N	0.103461	-0.370376	-1.261329
10 H	0.853335	0.310934	-1.395460

11	C	-0.507726	2.891021	0.197412
12	C	0.384829	3.989711	0.440768
13	H	0.173989	5.020855	0.188549
14	C	1.493050	3.474319	1.031638
15	H	2.382841	3.991938	1.365165
16	C	1.281677	2.059514	1.144726
17	C	2.200827	1.175340	1.681774
18	C	2.015221	-0.193202	1.756089
19	C	2.979008	-1.114319	2.290266
20	H	3.940432	-0.829911	2.697391
21	C	2.443989	-2.355548	2.169047
22	H	2.872023	-3.305180	2.462442
23	C	1.148304	-2.193795	1.568231
24	C	0.281401	-3.238090	1.296323
25	C	-0.985301	-3.096639	0.755722
26	C	-1.880418	-4.194566	0.516256
27	H	-1.648015	-5.232726	0.714915
28	C	-3.026127	-3.666350	0.016817
29	H	-3.929848	-4.178930	-0.285537
30	C	-2.829606	-2.246297	-0.057780
31	C	-3.780103	-1.356452	-0.525172
32	C	-3.583722	0.008284	-0.634354
33	C	-4.557263	0.934558	-1.134947
34	H	-5.551418	0.663215	-1.465050
35	C	-3.981496	2.164795	-1.107743
36	H	-4.405414	3.112359	-1.413557
37	C	-2.656665	1.994934	-0.582879
38	C	-1.762494	3.029503	-0.371224
39	H	0.533490	-1.296336	-1.271127
40	H	-2.330181	-0.494707	2.500738
41	H	-1.948895	1.104692	2.423296
42	H	3.133772	1.581446	2.058746
43	H	0.612844	-4.242624	1.538438
44	H	-4.737867	-1.756949	-0.840620
45	H	-2.076002	4.029244	-0.653717
46	H	-0.876130	0.035087	3.065319

Table S16: *OH-down*-(por)$Fe^{II}(H_2O_2)(NH_3)$

ATOM		X	Y	Z
1	Fe	-0.050356	0.012191	0.100478
2	O	1.119312	-0.064652	-2.672778
3	H	1.749464	-0.213991	-1.939177
4	N	-0.478309	-1.950880	0.063055
5	N	-2.006507	0.433856	0.044987
6	N	0.388215	1.963141	0.077920
7	N	1.920684	-0.420158	0.109275
8	N	-0.074945	0.041528	2.111892
9	O	-0.115529	-0.042193	-1.947343
10	H	-0.488620	-0.909617	-2.179450
11	C	0.411436	-2.992132	0.075223
12	C	-0.286289	-4.255795	0.067756
13	H	0.193461	-5.226586	0.069646
14	C	-1.612111	-3.967510	0.059488
15	H	-2.452213	-4.650763	0.052527
16	C	-1.721230	-2.528460	0.060449
17	C	-2.922154	-1.833049	0.057354
18	C	-3.049116	-0.450918	0.046490
19	C	-4.311748	0.250637	0.018587
20	H	-5.284123	-0.225807	0.011036
21	C	-4.017087	1.574029	-0.005515
22	H	-4.695809	2.417233	-0.036126
23	C	-2.576218	1.676073	0.012408
24	C	-1.878310	2.874742	0.002195
25	C	-0.497657	3.002163	0.030977
26	C	0.199530	4.268146	0.037669
27	H	-0.279996	5.238353	0.001820
28	C	1.522419	3.979774	0.095875
29	H	2.363721	4.661214	0.115716
30	C	1.627901	2.538406	0.120551
31	C	2.830591	1.849078	0.187186
32	C	2.965009	0.468367	0.193167
33	C	4.220147	-0.234926	0.267393
34	H	5.191669	0.239306	0.329275
35	C	3.927320	-1.561384	0.239296
36	H	4.608028	-2.402728	0.276284
37	C	2.493170	-1.668018	0.150249
38	C	1.793152	-2.865540	0.114957
39	H	-1.024017	-0.051411	2.470882
40	H	0.295446	0.921572	2.467796
41	H	-3.837764	-2.417959	0.054627
42	H	-2.461785	3.790810	-0.027889
43	H	3.742369	2.438137	0.231508

44	H	2.375395	-3.782623	0.133950
45	H	0.481360	-0.710361	2.514915

Table S17: *OH-down*-(por)$Fe^{III}(H_2O_2)(NH_3)$

ATOM		X	Y	Z
1	Fe	0.566594	-0.033287	0.563411
2	O	0.003841	-0.109177	3.484446
3	H	-0.725943	-0.524007	2.980410
4	N	1.398282	-1.839750	0.412478
5	N	2.347210	0.778961	0.225624
6	N	-0.258206	1.759362	0.765778
7	N	-1.213917	-0.857052	0.953368
8	N	0.167834	-0.020126	-1.366238
9	O	1.029130	-0.066037	2.501078
10	H	1.603531	-0.817310	2.733706
11	C	0.765299	-3.050738	0.581636
12	C	1.687945	-4.130196	0.370330
13	H	1.436242	-5.179479	0.453853
14	C	2.884145	-3.571864	0.052722
15	H	3.818906	-4.066570	-0.176234
16	C	2.698754	-2.149903	0.080624
17	C	3.698667	-1.226282	-0.164409
18	C	3.528376	0.142940	-0.078430
19	C	4.580907	1.101620	-0.266929
20	H	5.604950	0.851703	-0.511856
21	C	4.035346	2.326548	-0.062434
22	H	4.517480	3.294288	-0.106427
23	C	2.644984	2.119238	0.236587
24	C	1.746123	3.141644	0.477783
25	C	0.395514	2.965181	0.716449
26	C	-0.529857	4.047181	0.912819
27	H	-0.257878	5.094672	0.922645
28	C	-1.756790	3.491465	1.070252
29	H	-2.705080	3.985119	1.237386
30	C	-1.580321	2.068959	0.983806
31	C	-2.608006	1.152525	1.109539
32	C	-2.432859	-0.218994	1.088609
33	C	-3.482204	-1.179150	1.252801
34	H	-4.526740	-0.932422	1.391184
35	C	-2.904115	-2.409030	1.210025
36	H	-3.379220	-3.377320	1.299022
37	C	-1.499812	-2.206019	1.008708
38	C	-0.576692	-3.227441	0.868982
39	H	1.015577	0.124120	-1.914286
40	H	-0.488941	0.723793	-1.601212
41	H	4.685422	-1.600229	-0.416574
42	H	2.125731	4.157958	0.462643
43	H	-3.613791	1.533660	1.251951
44	H	-0.940284	-4.245901	0.958733
45	H	-0.246484	-0.904999	-1.658767

Table S18: *OH-down*-(TPP)Co^{II}(AmphNHOH)

ATOM		X	Y	Z
1	Co	0.402655	-0.058143	0.606407
2	O	0.825545	-1.012004	-2.363791
3	H	1.566022	-1.184047	-1.761607
4	N	-0.308352	-1.924886	0.731760
5	N	2.258215	-0.782785	0.435835
6	N	1.134175	1.794705	0.702069
7	N	-1.440806	0.657042	0.903037
8	N	0.019774	-0.108729	-1.616683
9	H	-0.890549	-0.569434	-1.584172
10	C	-1.608376	-2.307224	0.932465
11	C	-1.713449	-3.746431	0.962367
12	H	-2.625353	-4.301676	1.130409
13	C	-0.468267	-4.231499	0.747481
14	H	-0.150182	-5.263891	0.701843
15	C	0.401106	-3.089924	0.605330
16	C	1.772346	-3.195917	0.390722
17	C	2.631701	-2.100983	0.338021
18	C	4.060958	-2.210661	0.195459
19	H	4.605882	-3.138978	0.095633
20	C	4.554704	-0.949177	0.238573
21	H	5.587546	-0.634381	0.184069
22	C	3.426659	-0.065273	0.387427
23	C	3.539465	1.319713	0.488248
24	C	2.450084	2.173014	0.644313
25	C	2.564576	3.610594	0.671944

26	H	3.493887	4.161747	0.639466
27	C	1.303476	4.099703	0.732657
28	H	0.988275	5.133126	0.772448
29	C	0.418097	2.961230	0.747766
30	C	-0.969906	3.068961	0.806984
31	C	-1.823943	1.972460	0.900536
32	C	-3.257043	2.082226	1.017825
33	H	-3.813236	3.009221	1.020965
34	C	-3.736385	0.820178	1.110978
35	H	-4.765258	0.500619	1.197720
36	C	-2.599349	-0.062940	1.035871
37	C	-2.700718	-1.452310	1.068062
38	C	2.358336	-4.561234	0.226125
39	C	2.296356	-5.207379	-1.011469
40	H	1.817500	-4.705748	-1.848675
41	C	2.840532	-6.480352	-1.171828
42	H	2.788307	-6.972204	-2.139143
43	C	3.450923	-7.120803	-0.094372
44	H	3.875343	-8.113220	-0.218019
45	C	3.514863	-6.482853	1.143568
46	H	3.987270	-6.975983	1.988533
47	C	2.971123	-5.209593	1.302043
48	H	3.016700	-4.708985	2.265772
49	C	4.901308	1.926121	0.385987
50	C	5.529500	2.036265	-0.858065
51	H	5.016844	1.671269	-1.744450
52	C	6.796451	2.605918	-0.964176
53	H	7.273273	2.684193	-1.937287
54	C	7.449407	3.074405	0.175128
55	H	8.436528	3.520829	0.094451
56	C	6.829271	2.969087	1.419127
57	H	7.330837	3.333234	2.311388
58	C	5.562371	2.397796	1.523389
59	H	5.075472	2.316331	2.491763
60	C	-1.574240	4.434441	0.765032
61	C	-1.626951	5.140309	-0.440673
62	H	-1.212782	4.687123	-1.338201
63	C	-2.196402	6.410610	-0.496162
64	H	-2.230124	6.946151	-1.440792
65	C	-2.720682	6.991224	0.657794
66	H	-3.167216	7.980647	0.616975
67	C	-2.669468	6.295886	1.864999
68	H	-3.074056	6.742413	2.769021
69	C	-2.099176	5.025657	1.917733
70	H	-2.058872	4.481743	2.857801
71	C	-4.055076	-2.057652	1.244642
72	C	-4.688149	-2.698897	0.175783
73	H	-4.180992	-2.746937	-0.783296
74	C	-5.954250	-3.257624	0.333702
75	H	-6.434782	-3.749550	-0.507786
76	C	-6.603078	-3.183053	1.565481
77	H	-7.590477	-3.619157	1.688872
78	C	-5.977186	-2.549165	2.637863
79	H	-6.474108	-2.492625	3.602344
80	C	-4.710883	-1.989776	2.477351
81	H	-4.221229	-1.496380	3.312893
82	C	-0.132687	1.154829	-2.357114
83	H	-0.663373	1.803280	-1.649746
84	C	1.222149	1.769975	-2.677296
85	H	1.856286	1.793933	-1.788540
86	H	1.088448	2.798402	-3.029612
87	H	1.735587	1.200975	-3.458447
88	C	-1.004790	0.995634	-3.616383
89	H	-1.077111	1.974697	-4.107310
90	H	-0.498270	0.320771	-4.316106
91	C	-2.385228	0.477540	-3.289263
92	C	-2.773558	-0.820316	-3.634373
93	H	-2.080092	-1.457193	-4.178875
94	C	-4.034999	-1.304228	-3.287636
95	H	-4.319265	-2.315575	-3.567274
96	C	-4.923209	-0.498341	-2.579554
97	H	-5.900284	-0.877576	-2.293813
98	C	-4.542172	0.793242	-2.219789
99	H	-5.218426	1.423623	-1.650101
100	C	-3.285272	1.273739	-2.571962
101	H	-2.993958	2.278793	-2.272041

Table S19: *OH-up*-(TPP)Co^{II}(AmphNHOH)

ATOM	X	Y	Z
1 Co	-0.439536	-0.068818	-0.631349
2 O	-0.210875	-1.365935	2.253227
3 H	0.474295	-1.544709	2.918810

4	N	0.436518	-1.852400	-0.842907
5	N	-2.211144	-0.945153	-0.455344
6	N	-1.325040	1.720568	-0.608706
7	N	1.326260	0.825264	-0.967121
8	N	0.181997	-0.194452	1.558472
9	H	1.165696	-0.321573	1.315031
10	C	1.763885	-2.108932	-1.060428
11	C	2.014155	-3.530169	-1.037036
12	H	2.976689	-3.996653	-1.194518
13	C	0.827971	-4.127750	-0.773697
14	H	0.621281	-5.183603	-0.667288
15	C	-0.150247	-3.073928	-0.659495
16	C	-1.500100	-3.299760	-0.404226
17	C	-2.453096	-2.287392	-0.348499
18	C	-3.869094	-2.537908	-0.223548
19	H	-4.323252	-3.515530	-0.140760
20	C	-4.482075	-1.332137	-0.266875
21	H	-5.540857	-1.117882	-0.221847
22	C	-3.438860	-0.343049	-0.396190
23	C	-3.678382	1.028632	-0.427785
24	C	-2.666070	1.981539	-0.507382
25	C	-2.900233	3.401574	-0.412284
26	H	-3.871149	3.867550	-0.317046
27	C	-1.685477	3.999396	-0.448583
28	H	-1.456709	5.055007	-0.395114
29	C	-0.711026	2.946460	-0.590681
30	C	0.654439	3.178809	-0.723988
31	C	1.588706	2.169901	-0.945507
32	C	2.985659	2.418063	-1.196941
33	H	3.446317	3.395688	-1.239035
34	C	3.569153	1.207390	-1.370364
35	H	4.608185	0.989553	-1.576286
36	C	2.531930	0.219505	-1.214688
37	C	2.761570	-1.154136	-1.249229
38	C	-1.957952	-4.703902	-0.180798
39	C	-2.244881	-5.141977	1.115631
40	H	-2.122999	-4.448941	1.943942
41	C	-2.679855	-6.446010	1.342089
42	H	-2.899855	-6.772585	2.354822
43	C	-2.833819	-7.327427	0.272842
44	H	-3.173329	-8.344408	0.448372
45	C	-2.549992	-6.897971	-1.022813
46	H	-2.671164	-7.578663	-1.860889
47	C	-2.113908	-5.593469	-1.247559
48	H	-1.893630	-5.256314	-2.257209
49	C	-5.089476	1.510060	-0.337564
50	C	-5.774919	1.483538	0.880477
51	H	-5.271748	1.097578	1.763348
52	C	-7.086941	1.944989	0.965289
53	H	-7.607020	1.921168	1.918877
54	C	-7.729321	2.439301	-0.169163
55	H	-8.751595	2.801156	-0.103612
56	C	-7.053287	2.468329	-1.387815
57	H	-7.545861	2.852274	-2.276804
58	C	-5.741139	2.006580	-1.470255
59	H	-5.210648	2.028155	-2.418583
60	C	1.146891	4.588713	-0.659184
61	C	1.626766	5.112685	0.544254
62	H	1.626273	4.488568	1.434837
63	C	2.097436	6.422646	0.611121
64	H	2.469149	6.816319	1.553112
65	C	2.093417	7.224452	-0.529346
66	H	2.462826	8.244881	-0.479936
67	C	1.614345	6.710611	-1.733681
68	H	1.608416	7.328623	-2.627257
69	C	1.144074	5.400343	-1.797091
70	H	0.769483	4.996157	-2.733979
71	C	4.164818	-1.628652	-1.444504
72	C	4.901373	-2.096167	-0.351920
73	H	4.436469	-2.108318	0.630049
74	C	6.212468	-2.536149	-0.516675
75	H	6.771786	-2.898204	0.341974
76	C	6.803684	-2.512841	-1.779188
77	H	7.826246	-2.855739	-1.909925
78	C	6.075600	-2.049682	-2.874091
79	H	6.529751	-2.032064	-3.860921
80	C	4.763112	-1.610656	-2.707110
81	H	4.193002	-1.250951	-3.559703
82	C	0.049881	1.006967	2.393594
83	H	0.356985	1.814601	1.718731
84	C	-1.403065	1.226965	2.791291
85	H	-2.042575	1.229924	1.906486
86	H	-1.508480	2.189586	3.303135
87	H	-1.745726	0.434019	3.463518
88	C	0.982978	1.008738	3.623492
89	H	0.973214	2.020718	4.048256

90	H	0.570902	0.352268	4.401247
91	C	2.400985	0.591463	3.303244
92	C	2.999253	-0.484225	3.965867
93	H	2.449001	-1.005111	4.748010
94	C	4.299535	-0.887161	3.656882
95	H	4.745884	-1.723907	4.187237
96	C	5.018845	-0.219960	2.669406
97	H	6.028797	-0.531706	2.418718
98	C	4.428562	0.845358	1.990351
99	H	4.970195	1.358915	1.202164
100	C	3.134105	1.246120	2.304407
101	H	2.686781	2.069157	1.751112